Award Number: W81XWH-12-2-0120

TITLE: Early Diagnosis and Intervention Strategies for Post-Traumatic Heterotopic Ossification in Severely Injured Extremities

PRINCIPAL INVESTIGATOR:
Dr. Jonathan Forsberg

CONTRACTING ORGANIZATION: The Geneva Foundation
Tacoma, WA 98402

REPORT DATE: December 2016

TYPE OF REPORT: Final

PREPARED FOR: U.S. Army Medical Research and Materiel Command
Fort Detrick, Maryland 21702-5012

REPORT DOCUMENTATION PAGE					*Form Approved* *OMB No. 0704-0188*
Public reporting burden for this collection of information is estimated to average 1 hour per response, including the time for reviewing instructions, searching existing data sources, gathering and maintaining the data needed, and completing and reviewing this collection of information. Send comments regarding this burden estimate or any other aspect of this collection of information, including suggestions for reducing this burden to Department of Defense, Washington Headquarters Services, Directorate for Information Operations and Reports (0704-0188), 1215 Jefferson Davis Highway, Suite 1204, Arlington, VA 22202-4302. Respondents should be aware that notwithstanding any other provision of law, no person shall be subject to any penalty for failing to comply with a collection of information if it does not display a currently valid OMB control number. **PLEASE DO NOT RETURN YOUR FORM TO THE ABOVE ADDRESS.**					
1. REPORT DATE December-2016		**2. REPORT TYPE** Final			**3. DATES COVERED** 30Sep2012 - 29Sep2016
4. TITLE AND SUBTITLE Early Diagnosis and Intervention Strategies for Post-Traumatic Heterotopic Ossification in Severely Injured Extremities					**5a. CONTRACT NUMBER** **5b. GRANT NUMBER** W81XWH-12-2-0120 **5c. PROGRAM ELEMENT NUMBER**
6. AUTHOR(S) Dr. Jonathan Forsberg, Dr. George Muschler, Dr. Thomas Davis E-Mail(s): muschlg@ccf.org; jonathan.a.forsberg.mil@health.mil; thomas.a.davis196.ctr@mail.mil					**5d. PROJECT NUMBER** **5e. TASK NUMBER** **5f. WORK UNIT NUMBER**
7. PERFORMING ORGANIZATION NAME(S) AND ADDRESS(ES) AND ADDRESS(ES) The Geneva Foundation 917 Pacific Avenue Tacoma, WA 98402 The Cleveland Clinic 9500 Euclid Avenue Cleveland, OH 44195					**8. PERFORMING ORGANIZATION REPORT**
9. SPONSORING / MONITORING AGENCY NAME(S) AND ADDRESS(ES) U.S. Army Medical Research and Materiel Command Fort Detrick, Maryland 21702-5012					**10. SPONSOR/MONITOR'S ACRONYM(S)** **11. SPONSOR/MONITOR'S NUMBER(S)**
12. DISTRIBUTION / AVAILABILITY STATEMENT Approved for Public Release; Distribution Unlimited					
13. SUPPLEMENTARY NOTES					
14. ABSTRACT This study will recruit wounded warriors with severe extremity trauma, which places them at high risk for heterotopic ossification (HO); bone formation at abnormal sites, which causes pain, limits motion and/or limits the use of a prosthetic device. There are three goals: 1) to understand the mechanisms involved in HO; 2) to define accurate and practical methods to predict where HO will develop; and 3) to define potential therapies for prevention or mitigation of HO.					
15. SUBJECT TERMS Wound healing					
16. SECURITY CLASSIFICATION OF:			**17. LIMITATION OF ABSTRACT**	**18. NUMBER OF PAGES**	**19a. NAME OF RESPONSIBLE PERSON** USAMRMC
a. REPORT U	**b. ABSTRACT** U	**c. THIS PAGE** U	UU	5 3	**19b. TELEPHONE NUMBER** *(include area code)*

Table of Contents

Page

1. INTRODUCTION

The mechanism(s) involved in heterotopic ossification (HO) in our severely injured wounded warriors are unclear. Accurate, practical methods and assessment tools (macroscopic and cellular/molecular) need to be developed to characterize wounded tissues and predict where HO may or will develop. These tools need to provide insight into the biological wound environment and events that contribute to or elicit HO. These tools also need to provide effective methods for early diagnosis or risk assessment (prediction) so that therapies for prevention or mitigation of HO can be optimally targeted. This study seeks to contribute to advancement in each of these key areas.

Major specific aims and project tasks of the research proposal:

Specific Aim 1: Characterize the heterogeneity and evolution of the biological environment in exposed tissue sites in wounded warriors under treatment for traumatic amputations of the lower extremity between week 1 and week 4 following injury using multiple modalities: (*time frame 1-33 months*)

Tasks

a. Human Use regulatory review and approval by US Army Medical Research and Material Command (USAMRMC) Office of Research Protection (ORP) and the local Walter Reed National Military Medical Center IRB (*WRNMMC; time frame: months 1-3*)

b. Enroll five (5) patient subjects with major limb amputation proximal to the ankle or wrist joint. The predilection of HO in combat amputees has been well studied; HO develops in the majority of combat-related amputations. (*WRNMMC; time fame: months 25-33*).

c. Analysis of serum and wound fluid for growth factors and inflammatory cytokines (leverage from other funded work (*WRNMMC; time frame: 25-33 months*)

d. Analysis of biopsied tissue for gene mRNA transcripts involved in early osteogenic cell development, proliferation and differentiation (n =60 samples at three debridement points; *NMRC; time frame: months 25-33*)

e. Assay of the concentration, prevalence, heterogeneity and biological potential of connective tissue progenitors (CTPs), including osteogenic CTPs (CTP-Os) (n = 240 images of 60 cultured tissue samples; NMRC & *CCLRI; time frame: 25-33 months*)

f. Cryopreservation of muscle-derived nucleated cells for use in Specific Aim 3 studies. (*NMRC; time frame months 25-33*)

g. Noninvasive digital photography of wounds and computer-based software planimetry analysis of digital images (wound mapping) at all debridement time points until definitive wound closure (*WRNMMC; time frame: months 25-33*)

h. Standard histopathological assessment (H&E, Masson's trichrome and IHC) of collected tissues (*n*=60 tissue samples; NMRC, *time frame months 25-33*)

i. Collection and the image analysis of topical high resolution ultrasound (HRUS) images of various anatomical sites within each wound. Acquire high-frequency ultrasound acquisition signals from each image which will be processed using instrumentation specific software algorithms for the development of a "virtual histology" imaging technique *(WRNMMC and CCLRI, time frame months 25-33*).

j. Collect Raman spectra of biopsied tissues collected from various anatomical sites within each wound. Topical Raman Spectroscopy (leverage from other funded work; *WRNMMC; time frame: months 25-33*)

Specific Aim 2: Develop a predictive model based on a minimum set of clinical variables collected in Aim 1, that will provide clinically useful prediction of where and in whom HO will form. (25-36 months)

Tasks

a. Correlate/compare CTP results, Raman spectra, ultrasound virtual histology images, osteogenic/mesenchymal /inflammatory gene transcript expression findings, and serum/wound effluent results with histopathology observations, radiographic/CT results, patient demographic data and with physician observations using Bayesian Modeling. Interactions between variables will be assessed. (*NMRC; time frame months 33-36*)

b. Correlate processed ultrasound and Raman images with standard histopathological findings (*WRNMMC; time frame: months 25-36*)

c. Correlate the concentration and prevalence of CTP-O progenitor cells with osteogenic gene expression and Raman spectroscopic markers (*NMRC; time frame: months 25-36*).

d. Using Bayesian modeling, validate and correlate cellular, molecular and imaging results with patient HO outcome as a predictor (*NMRC; time frame months 25-36*).

Specific Aim 3: Identify one or more potential local or topical therapeutic agents that effectively inhibit colony formation, proliferation, differentiation and/or survival of CTP-Os in vitro that could be tested in a subsequent clinical trial. (1-36 months)

Tasks

a. Qualitatively assess the effect of each agent under conditions in which the agent is present throughout the culture period to define the effect and the preferred *in vitro* dose or dose range for each agent. (*CCLRI; time frame months 25-36*)

b. Using a subset of active agents defined in task 3a, complete quantitative screening to assess the effect of agent dose and the effect of the timing and duration of exposure. (*CCLRI; time frame months 25-36*)

Specific Aim 4: Characterize the heterogeneity and evolution of the biological environment in tissue sites in traumatic amputations of the lower extremity in the Rat HO model between week 1 and week 3 following injury using multiple modalities.

Tasks

a. Animal Care and Use Committee approval NMRC and ACURO approval for animal protocol (NMRC*: time frame: months 27-29).*

b. Complete protocol on 65 rats. (NMRC*; time fame: months 30-32*).

c. Analysis of biopsied tissue for gene mRNA transcripts. NMRC*; time frame: months 31-33*).

d. Assay of the concentration, prevalence, heterogeneity and biological potential of connective tissue progenitors (CTPs), including osteogenic CTPs (CTP-Os) NMRC & CCLRI*; time frame: months 30-33*)

e. Standard histopathological assessment (H&E, Masson's trichrome and IHC) of collected tissues (*n*=65 tissue samples; NMRC, *time frame: months 30-33*)

f. Collect Raman spectra of biopsied tissues collected from various anatomical sites within each wound. Topical Raman Spectroscopy (leverage from other funded work; WRNMMC*; time frame:months 30-32*)

g. Correlate Raman images with standard histopathological findings (WRNMMC*; time frame: months 32-33*)

h. Correlate the concentration and prevalence of CTP-O progenitor cells with osteogenic gene expression and Raman spectroscopic markers (NMRC*; time frame months 32-33*).

i. Using Bayesian modeling, validate and correlate cellular, molecular and imaging results with patient HO outcome as a predictor *(*NMRC*; time frame:(2) months: 33-35, June to August, 2015).*

2. KEYWORDS

extremity trauma, fractures, heterotopic ossification, palovarotene, connective tissue progenitor cells, blast injury, combat-related injury, limb amputation, crush injury, gene expression, raman spectroscopy, wound healing, osteogeneisis, chondrogenesis, tissue regeneration, inhibitors of bone development.

3. OVERALL PROJECT SUMMARY

Specific Aim 1: Characterize the heterogeneity and evolution of the biological environment in exposed tissue sites in wounded warriors under treatment for traumatic amputations of the lower extremity between week 1 and week 4 following injury using multiple modalities.

Note that in the initial proposal, we projected that we may recruit up to 25 patients into this cohort. Fortunately, the frequency of these injuries has decreased from the time that the initial study was proposed. We adjusted to this change in frequency of these injuries by revising the study to reduce that number of projected patients from 25 to 5 and to add an Aim 4, to address these questions using a rat model for HO, as outlined above.

Given the limited power available from an assessment of this reduced patient cohort, the benefit of the work provided here is limited in terms of characterization, but significant in terms of laying the groundwork for systematic analysis of early stages of HO from the time of injury through the first radiographic evidence of HO using each of the modalities proposed: Radiographs, serum cytokines, cell and CTP analysis, histology, ultrasound and Raman Spectroscopy. Effective protocols for tissue sampling and analysis have been established, as well as the characteristics of the data set and range of data values that may be expected in clinical experience.

A. **Patient Demographics and Radiographic Imaging**:

Three combat wounded patients were enrolled in this study. A brief description of each patient's clinical history is provided below along with a plain film images of each wound site at approximately 3 months post injury.

Patient 1: Patient 1 is a 25 year old male who sustained a dismounted IED blast. His orthopedic injuries included a right acetabular fracture, right inferior/superior rami fractures, left SI dislocation (LC3), left traumatic below knee amputation which was converted to a through-knee disarticulation, a right open and comminuted tib/fib fracture with extensive soft tissue and popliteal artery injuries which was later converted to a right hip disarticulation, a right hand soft tissue injury and L4 and L5 transverse process fractures. His non-orthopedic injuries included: urethral injury, testicular rupture, penetrating abdominal injury, severe perineal and gluteal soft tissue injuries and a right iliac vessel injury s/p repair. Prior to arrival at Walter Reed he underwent I&D of all wounds, pelvic exfix and vessel repair on the day of injury. Repeat I&D and wound vac placement on post-injury day (PID) 1. Repeat I&D and R transfemoral amputation revision on PID 2 followed by repeat I&D on PID 3 and 4. Patient arrived at WR on PID 6. His injury severity score (ISS) was 32. His right hip disarticulation was the enrolled wound which was graded as a GA IIIA measuring 41cm x 21cm x 15cm. Heterotopic ossification was first identified at the 1 month follow-up visit and was given a HO grade 1 and at the 3 month visit remained a grade 1.

Patient 2: Patient is a 29 year old male who sustained a dismounted IED blast. His orthopedic injuries included a traumatic left through knee amputation, a comminuted open right tibia fracture which was converted to a through knee amputation, pelvic fracture, left zone 2 sacral fracture, right SI joint widening and a right middle finger metacarpal base fracture. His non-orthopedic injuries included a large soft tissue injury through the right groin extending through the external sphincter treated using a colostomy, mild TBI and Enterobacter pneumonia. A pelvic ex-fix was place on the day of injury. Prior to arrival at Walter Reed, he underwent a rectosigmoid transection and diversion without ostomy and tying off

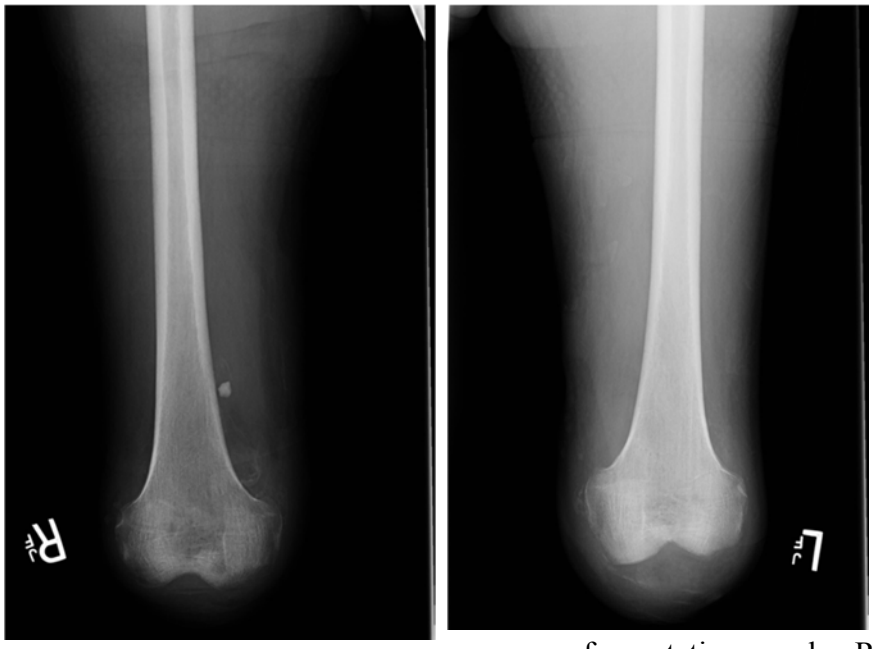

of prostatic vessels, RLE through knee amputation with patellectomy and left amputation revision. On PID 4 he underwent BLE I&D and wound vac exchange. He arrived at WR on PID 5. His ISS was 18. The right knee disarticulation was enrolled as wound 1 which measured 15cm x 22cm x 8cm. The left knee disarticulation was enrolled as wound 2 which measured 28cm x 15cm 8cm. Heterotopic ossification was first identified at the 1 month follow-up and was given a HO grade 1 in both wounds and remained as a 1 at 3 month follow-up.

Patient 3: Patient is a 45 year old male who sustained a dismounted IED blast. His orthopedic injuries included a right traumatic below knee amputation, a left traumatic below knee amputation that was converted to a through knee amputation and an APC 3 pelvic fracture s/p ex-fix placement. His non-orthopedic injuries included a left thigh soft tissue injury, right pneumothorax s/p needle decompression followed by chest tube placement, a scrotal lac with injury to bilateral testes s/p temporary repair and closure as well as hypovolemic shock and acidosis s/p resuscitation. Prior to arrival at Walter Reed he underwent a massive transfusion w/ 15pRBC/13FFP/3plt, pelvic ex-fix placement, revision and I&D or traumatic amputations and a right knee arthrotomy and I&D on the day of injury. On PID 1 he underwent a pelvic ex-fix revision, I&D of BLE and his right hand as well as a wound vac placement to bilateral lower extremities. His ISS was 14. His right trans-tibial amputation was enrolled as wound 1 and measured 17cm x 12cm x 12cm. The left knee disarticulation was enrolled as wound 2 and measured 18cm x 22cm x 4cm. Heterotopic ossification was first identified at the 1 month follow-up and was graded as a 2 in wound 1 (right below knee amputation) and remained as a 2 at the last graded follow-up which was at 2 months.

Based on plain film radiographs and uCT imaging each wound biopsy site was examined by two orthopaedic surgeons blinded to the study for the presence or absence of ectopic bone formation at the indicated time points post injury (**Table 1.**).

Table 1. Incidence of HO at distinct biopsy sites determined by evidence of radiographic ectopic bone

	Time point (months)	Site 1	Site 2	Site 3	Site 4	Site 5	Site 6	Site 7	Site 8
Patient 1	1	HO+	HO-	HO-	HO-				
	2	HO+	HO+	HO-	HO+				
	3	HO+	HO+	HO-	HO+				
Patient 2	1	HO+	HO+	HO-	HO+	HO+	HO+	HO+	HO+
	2	-	HO+	HO-	HO+	-	-	HO+	-
	3	HO+	HO+	HO-	HO+	HO-	HO-	HO+	HO-
Patient 3	1	HO+	HO+	HO+	N/A	HO-	HO-	HO-	HO-
	2	HO+	HO+	HO+	N/A	HO-	HO-	HO-	HO-
	3	HO+	HO+	HO+	N/A	HO-	HO-	HO-	HO-

- Patient #1 had one wound wherein 1 out of 4 biopsied sites had visual radiographic evidence of bone formation by 1-month post injury.
- Patient #2 had two wounds wherein 7 out of 8 biopsied sites had visual radiographic evidence of bone formation by 1-month post injury.
- Patient #3 had two wounds wherein 3 out 4 biopsied sites in one wound and none of the biopsied sites in the other wound had visual radiographic evidence of bone formation by 1-month post injury

B. Systemic Inflammatory Response

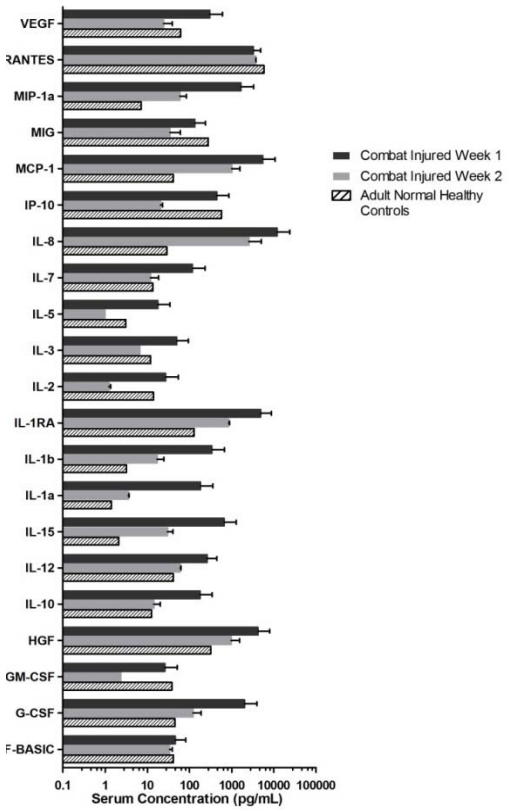

Figure 1. Comparison of Serum Cytokine Concentration Assays at 1 and 2 weeks are compared with serum levels measured in normal non-traumatized human subjects.

Methods: Peripheral venous blood (8 mL) was drawn prior to each surgical debridement. Wound effluent samples (>=30 mL) were collected from the VAC canister (without gel pack; Kinetic Concepts, Inc., San Antonio, TX) 2 hours following the first surgical debridement and over a 12 hour period prior to each subsequent wound debridement. All serum samples were immediately separated using a centrifuge at 2500 g for 10 minutes. Serum supernatants and effluent samples were transferred to individually labeled Cryo-Loc polypropylene tubes (Lake Charles Manufacturing, Lake Charles, LA) and flash-frozen in liquid nitrogen and stored at -80°C until analysis. Serum and wound effluent proteins were quantitated using a Luminex 100 IS xMAP Bead Array Platform (Millipore Corp, Billerica, MA) as described previously.13 Twenty-two cytokines and chemokines (interleukin [IL]-1[alpha], IL-1[beta], IL-2, IL-3, IL-4, IL-5, IL-6, IL-7, IL-8, IL-10, IL-12(p40), IL-12(p70), IL-13, IL-15, inducible protein [IP]-10, Eotaxin, interferon-[gamma], granulocyte macrophage-colony stimulating factor [GM-CSF], MCP-1, MIP-1[alpha], RANTES, and tumor necrosis factor-[alpha]) were quantified using Beadlyte Human 22-Plex Multi-Cytokine Detection System (Upstate/Millipore; Cat 48–011). Results were compared to cytokine levels in serum of healthy Subjects published in the journal of Mediators of Inflammation (Kleiner et al, 2013:434010. doi: 10.1155/2013/434010)

Results: Severe trauma induces an initial systemic inflammatory response, also known as systemic inflammatory response syndrome (SIRS). The physiologic response to acute traumatic injury in the 3 enrolled blast-related extremity injured patients was reflected in the serum and wound effluent protein cytokine and chemokine data (Figures 1. and 2.). We examined the total inflammatory mediator production across the first two weeks post admission in CONUS. The overall analysis of systemic inflammation biomarkers at the first week debridement time (3-6 days post injury; Figure 1.)) and 2 week debridement time (8-12 days post injury; Figure 2.) showed that circulating levels of VEGF, MIPα, MCP-1, IL-8, IL-7, IL-5, IL-3, IL-1ra, IL-1β, IL-1α, IL-15, IL-12, IL-10, HGF, and G-CSF were markedly higher in combat-injured patients, when compared with normal healthy control subjects. There was a trend for to see a decrease in these values between week 1 and 2 post injury. Only GM-CSF and IL- MIG and RANTES were not significantly elevated.

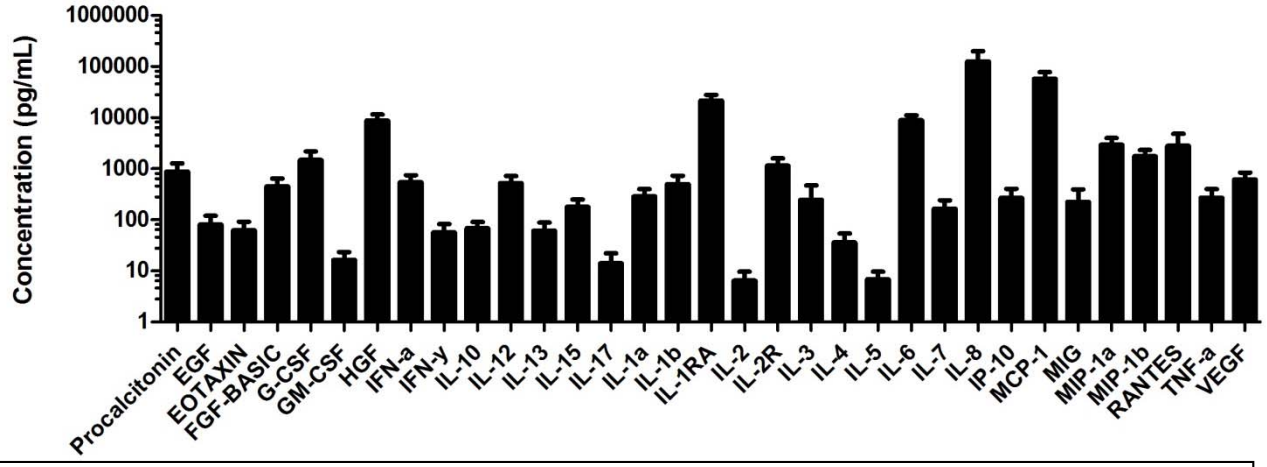

Figure 2: Wound tissue associated inflammatory mediators detected in wound effluent collected from patient following combat blast-related extremity trauma. Results combined from collection at 3-6 days post injury (1 week, n = 3 patients; 5 wounds) and 8-12 days post injury (n = 2 patient; 2 wounds).

It was not possible to test the hypothesis that serum cytokine levels could be used to predict HO development. Not only was there a small number of patients (n= 3, 5 total wounds), all three patients had at least one wound that developed HO. Moreover, only a single wound in patient-3 healed without HO development.

C. **Quantification of osteoblastic connective tissue progenitor cells (CTP-Os)**.

Methods: Muscle tissue samples (0.1-0.5g) collected in the operating at the end of debridement procedures. Four sites were samples per wound from each wound (5 wounds in 3 patients). Each sample was immediately placed in cold (4ºC) Eagle medium (α-MEM) supplemented with antibiotics (100U/mL penicillin, 100ug/ml streptomycin; Invitrogen, Rockville, MD). Within 4 h of harvest the fascia and fat were microdissected from the tissue. The remaining muscle tissue sample was weighed, minced into a fine slurry using sterile scissors, and incubated in 300U/ml Collagenase Type II (Worthington, Lakewood, NJ) for 2 h. Samples were drawn repeatedly (10-15x) through a 5 ml pipette to breakup large tissue fragments and release cells, and then washed to remove cell debris. The centrifuged cell pellet was resuspended in complete human Mesenchymal Growth Medium (PT-3001; Lonza, Walkersville, MD) with antibiotics. Enzymatically extracted cells were filtered through 100-μm and 70-μm nylon strainers in order to remove muscle fibers and other debris, and were then washed and resuspended in osteogenic medium consisting of alpha-minimum essential medium Eagle (α-MEM) with 10% fetal bovine serum, 100 U/mL penicillin, 100μg/mL streptomycin, 10^{-8} M dexamethasone, and 50 μg/mL ascorbate. Cell suspensions were counted using a cellometer (Nexcelom Biosciences, St. Lawrence, MA). Cells were plated at a density of 250-4,000 cells/chamber (4.2 cm2; Labtek chamber slides)with medium changes on days 1, 3 and 5. Cultures were maintained in a controlled proOx-C-chamber system (C-Chamber, C-374; Biospherix, Redfield, NY). The oxygen concentration in three separate culture chambers were maintained at either 0.3%, 3%, or 21% with the residual gas mixture composed of 5% CO_2 and balance nitrogen for the duration of the experiments. Day 6 cultures were fixed with 1:1 acetone:methanol

for 10 min and stained for nuclei (4,6-diamidino-2-phenylindole [DAPI]) and alkaline phosphatase (AP) as a marker for the preosteoblastic activity. Chambers were scanned and analyzed using Colonyze™ software, identifying colonies containing eight or more cells in a cluster. CTP-O prevalence (pCTP-0) was defined as the number of CTP-Os per 10^6 cells plated. Total CTP concentration was defined as the number of CTP-Os per gram of muscle tissue.

Results:

- Muscle-derived nucleated cells were isolated and cultured for 6 days at various oxygen tensions and under culture conditions promoting the osteogenic differentiation of connective tissue progenitor cells (CTPs) in all samples.

- The number of CTP colonies per 1 x 10^6 viable cell plated was determined ("prevalence'). (Figure 3.)
- The concentration of CTPs per gram of tissue ("total CTP yield") was calculated based on the cell yield/gram of tissue times the prevalence.

- These values in injured/regenerative muscle varied significantly between patients, tissue samples and oxygen tension culture conditions.

- These data did not suggest clear differences in cellularity, CTP concentration or CTP prevalence between sites that developed HO versus those that did not.
- More patient samples and a more extensive study would be needed to be able to conclude the consequences of hypoxic conditions.

- Colony forming efficiency (CFU) among the muscle-derived progenitor population was greater when samples were cultured under 21% O_2 tension, but these data were not statistically significant.

- Of interests, when comparing to HO negative sites and positive sites, we observe an increasing but non-significant trend towards a higher colony forming efficiency prevalence in the 21% O_2 tension in the HO positive sites. (Figure 4.)

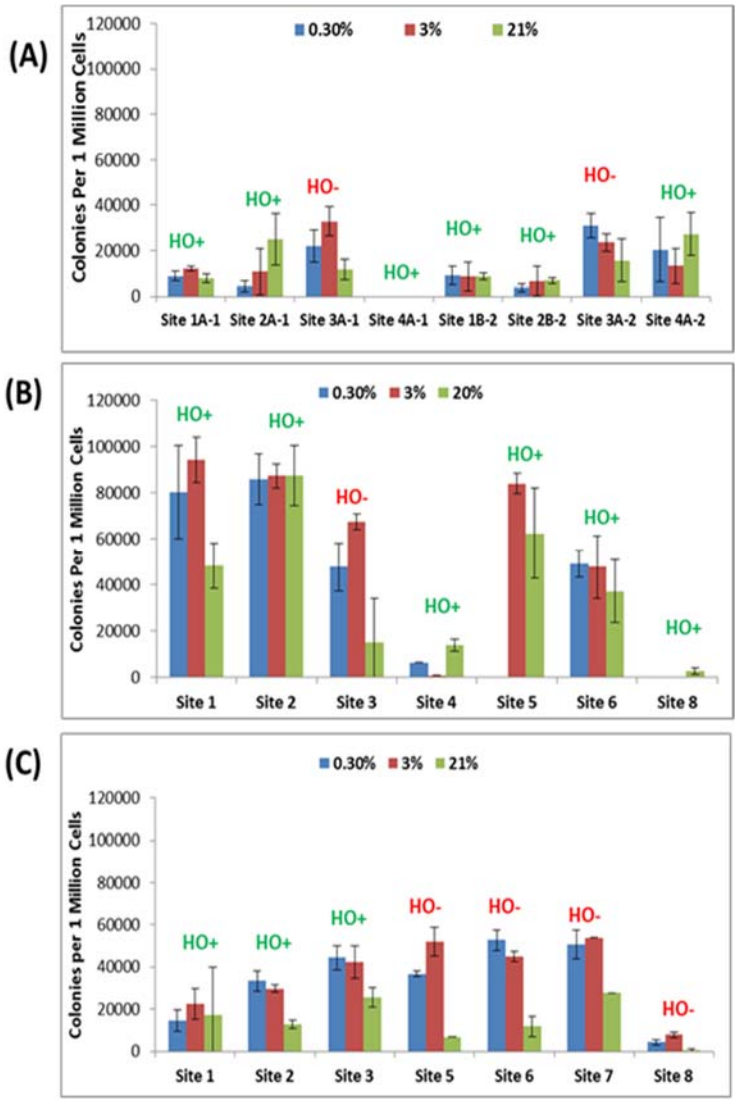

Figure 3. CTP Prevalence data for wound site muscle biopsy samples cultured at three oxygen tensions, Patients 1-3 (A,B,C) respectively, day 6 harvest.

D. Osteogenic Gene Expression Patterns following Trauma-induced HO Formation

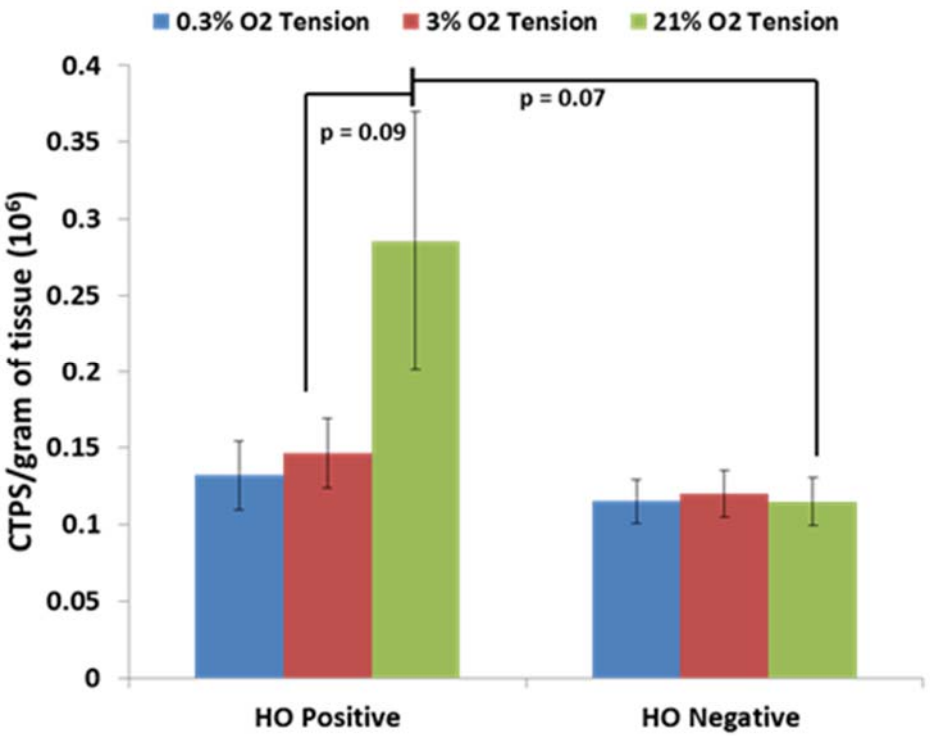

Figure 4. Total number of osteoblastic connective tissue progenitor cells (CTP-O) per gram of injured muscle tissue

At indicated debridement time points, a sample of skeletal muscle tissue collected from each identified biopsy site on each enrolled extremity wound (n = 5 wounds amongst 3 patients were stored in RNALater (Ambion Inc, Austin, TX, USA) at 4ºC. Total RNA was isolated and purified muscle cell lysates using RNeasy columns and DNase-I kits (Qiagen, Valencia, CA, USA) according to the manufacturer's protocols. RNA was stored at –80°C in nuclease-free water (Bio-Rad, Hercules, CA, USA). Total RNA was quantified spectroscopically by using NanoDrop 1000 (ThermoFisher Scientific, Waltham, MA) and RNA integrity/quality was assessed by microcapillary electrophoresis using an Agilent 2100 Bioanalyzer (Agilent Technologies, Santa Clara, CA). Reverse transcriptase polymerase chain reaction (RT-PCR) was used to convert 1 µg of RNA to cDNA. mRNA transcripts for 83 key genes involved in early chondrogenic, osteogenic and angiogenic signaling pathways (see Appendix 1 for the complete list of genes and their function) were examined by real-time PCR using a custom low density microarray (Bio-Rad Laboratories, Hercules, CA). Relative gene transcript expression was calculated using the $2^{-\Delta\Delta Ct}$ method and normalized and compared to the gene expression levels of non-injured muscle tissue collected from three non-trauma patients. Gene transcripts values that were significantly deferentially expressed between treatment groups are reported.

- We isolated RNA from the soft tissue biopsies from all the sites listed in Table 1, converted them into cDNA and ran qRT-PCR to study the changes in localized levels of osteogenic, angiogenic and chondrogenic genes.
- Multiple analyses of qRT-PCR data were conducted to identify the gene transcripts either across three patients, their HO classification (HO positive vs HO negative) or over time (Week 1 vs Week 2).
- In Patient #3 were we could compare four biopsy sites which were negative to four that were positive, there were genes that appeared to be differentially expressed (Table 2.). However, this hypothesis that relatively levels of gene expression could be used to predict HO formation could not be tested in this very limited sample size.

Table 2: Mean relative fold difference in expression among HO+ and HO- sites in patient #3.

Gene Transcripts	HO Positive Sites*	HO Negative sites*	p Value
ALPL	13.4	6.1	0.03
IBSP	1.5	2.5	0.02
CXCL10	0.6	1.7	0.02
ENG	0.7	0.9	0.01
FGF1	0.2	0.4	0.04
FGF2	0.08	0.2	0.03
HDAC1	0.7	1	0.007
ITGAM	1.8	2.8	0.006
ITGAV	0.8	1.2	0.02
KDR	1.05	1.8	0.02
CCL2	0.7	1.4	0.004
CCL3	1.7	3	0.004
NOTCH1	0.5	0.6	0.002
PPARG	0.3	0.7	0.03
SMURF1	0.5	0.8	0.04
TNF	0.48	0.8	0.007

* relative fold change in comparison to normal injured muscle

E. Early Detection of Soft Tissue Mineralization and Ectopic Bone Formation in Clinical Biopsies using Raman Spectroscopy:

Thirty tissue biopsies collected from three patients were examined *ex vivo* via Raman Spectroscopy using a Kaiser Rxn1 PhAT probe 830 nm system (Kaiser Optical Systems, Inc., Ann Arbor, MI, USA) with 3 mm diameter excitation spot size. Dark subtracted and intensity-corrected spectra were acquired at 2-5 locations within each biopsy each using 2 second acquisitions and 25 accumulations under the cosmic ray removal function. Spectra were collected every 5 mm on front and back surfaces of each biopsy with fewer acquisitions for smaller biopsies. All processing of Raman data was performed in MATLAB® using custom-built scripts. Spectra were averaged per biopsy and smoothed using a seventh-order polynomial Savitzky-Golay filter. The contributions of adipose tissue and blood were removed from each spectrum using spectral subtraction and factor analysis extracted pure adipose and blood components. Pure components were obtained by conducting singular value decomposition (SVD) multivariate analysis of the total biopsy spectral data set to reduce dimensionality of the data and allow for extraction of underlying common chemical constituents contributing to the total spectral dataset. An appropriate number of loadings were selected using a Scree plot and 99% of data variance was contained within. Band target entropy minimization (BTEM) was performed on the reduced

data to extract estimated adipose and blood pure factors. Prior to spectral subtraction, biopsy spectra and pure component adipose and blood spectra were truncated to 600-1750 cm^{-1}, baseline subtracted using a fifth-order polynomial fitting routine, and normalized to the methyl/methylene scissoring band at 1445 cm^{-1} as a marker of total protein content. Resulting spectra were analyzed for molecular markers of alterations in tissue composition characteristic to abnormal tissue pathology. Spectroscopic signatures were compared with histological results and clinical HO status assigned by 2 orthopaedic surgeons' assessment of plain film radiographs at each wound biopsy site examined at 1, 2, and 3 months post injury. HO positive (HO+) status was assigned to sites with radiographic evidence HO occurrence within the clinical course of the study, and HO negative (HO-) to sites that did not exhibit evidence of HO throughout the entire course of the study.

Results:

Examination of blood and adipose subtracted Raman spectra of early tissue biopsies from wounded warrior patients under treatment for combat-related transfemoral amputations or hip disarticulations exhibited increased collagen deposition at HO+ wound sites. Reference spectra of type I collagen and control muscle tissue are shown in Figure 5. When compared to muscle,collagen spectra exhibit: increased hydroxyproline and proline content, increased/changes in Amide III band and decreased CH_2CH_2 wag bands both indicative of decreased helical and increased β–sheet/disordered protein secondary structure, and increased Amide I bandwidth and shift to higher frequency of the underlying band center. Raman detected collagen content is increased for all three patients at HO+ sites and correlates with the earliest radiographic evidence of HO formation (Figure 6.),

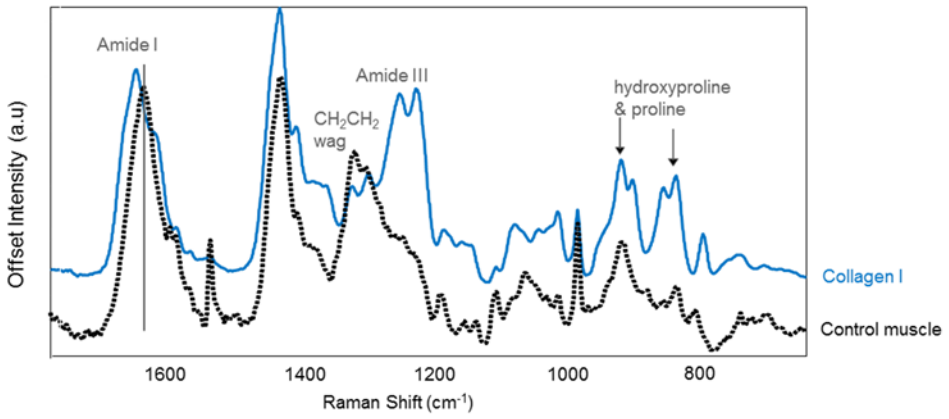

Figure 5. Example of Raman spectra of collagen I and uninjured muscle.

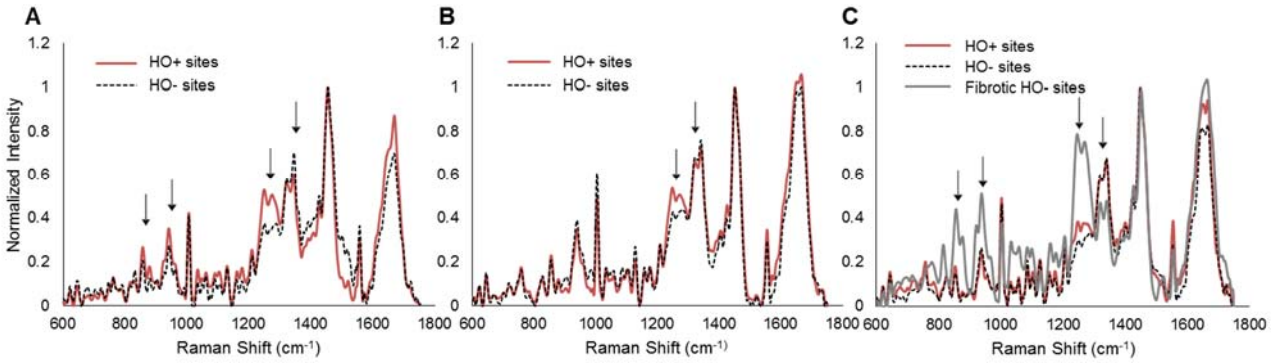

Figure 6. Mean Raman spectra of HO+ and HO- sites for A) Patient 1, B) Patient 2, C) Patient 3. Spectroscopic markers indicate increased biopsy collagen content for all three patients (arrows).

with the exception of two HO- sites (Patient 3) that exhibited high collagen spectral markers and correlated with highly fibrotic tissue pathology. This study demonstrates changes in collagen production as an early spectroscopic signature of HO in human tissue samples at time points prior to radiographic detection. Raman spectroscopy may serve as a tool for identifying and monitoring wound sites for altered collagen production and may inform future work for optimizing surgical excision at HO tissue margins and identifying highly fibrotic muscle regions.

F. High Resolution Ultrasound (HRUS)

Development of HO involves a process of change within the structure of the tissue. Ultrasound in general and spectral analysis specifically is able to provide distinction between differing structures. To investigate the ability of ultrasound to discern differences arising from HO, in-phase and quadrature (IQ) data were collected from three subjects at the following time points:

- Subject 1: sites 1-4 (single limb injury), Exam 1 & 2
- Subject 2: sites 1-8 (double limb injury), Exam 1 only
- Subject 3: sites 1-3,5-8 (double limb injury), Exam 1& 2

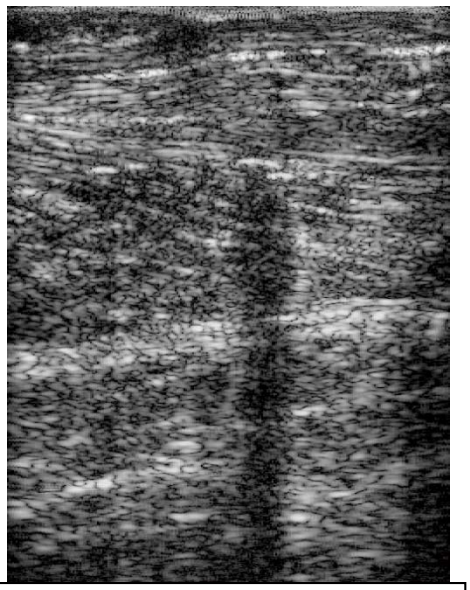

Figure 7.. Example of a bright feature with shadow present (arrow) . This is Subject 1 Site 2 in which HO did develop. Wound surface is on top and the image spans 3.85 cm wide by 5 cm deep with a focus at 1.3 cm.

At each site a Terason 2000 ultrasound system with a 10L5 probe was employed to capture the raw IQ data. The ultrasound probe was placed so that the imaging plane is parallel to a tangent of a circle centered on the femur. IQ data is collected while holding this probe still. IQ data while swiping the probe through this region is also collected while maintaining the same probe orientation.

For subjects with more than one Exam, images were compared in an attempt to locate the same positions within the tissue. However, this was not possible with any degree of confidence due to tissue loss associated with debridement procedures and tissue contraction scarring. In addition, the limited data sets (both in number of enrolled subjects and number of ultrasound Exams per subject) precluded the creation of a predictive model for HO based on analysis of ultrasonic data.

An alternate analysis was performed where the images were analyzed to look for bright reflecting areas with significant shadow in soft tissue regions. A observer blinded to the HO results provided in Table 3. viewed the

ultrasound images created from all of the collected IQ data. If the observer found a bright area followed by shadow (Figure 7.),at any time point then the site was considered to be positive for this test. The radiographic evidence for HO in Table 3. was used as the true state of HO at the site. This analysis demonstrated that the presence of a bright feature with shadow is insufficient and provided poor sensitivity or specificity as a test for HO. Accuracy of the test is 0.58 with sensitivity of 0.62 and specificity of 0.5. A possible reasons for false positive findings in an ultrasound based test are air bubbles or debris residing within the wound. For false negatives, may be expected prior to the generation of mineral deposits which should have a significant impact on US images.

Table 3: Matrix for predicting HO based on US images.

		Prediction from Ultrasound (Bright/Shadow Feature)	
		Positive	Negative
Actual HO (Radiographic)	Positive	8	5
	Negative	3	3

Application of spectral analysis techniques could provide an early indicator of the development of HO. However, the limited human data collected does not provide sufficient data to test this hypothesis.

The image analysis results do indicate that image based approaches which are sensitive to intensity of the backscattered ultrasound appear to be a poor test of HO development when used as a sole predictor. An improved approach would collect radiographic data (or other 'gold' standard) at the same time as the ultrasound data in a manner to insure matching between the two modalities.

G. Histological Assessment and Hyaluronan (HA) Staining

Background

Upon arrival at WRNMMC each patient begins a series of debridement procedures. These are usually continued three times per week until definitive wound closure using local tissue; flaps or skin grafts can also be attempted. Early debridement samples are usually obtained 6-8 days post injury. One wound presents up to four biopsy sites. Each sample was processed using fixation that would preserve HA and also allow all normal histochemical staining methods, particularly haematoxylin and eosin (H & E). All samples were stained in an outside reference lab for H & E.

All H&E stained patient biopsy samples for 3 patients (23 samples), were scanned and reviewed by two investigators, (CC). Sections were graded to estimate the percent tissue area defined by muscle, fat, fibrosis, hematoma and vasculature. Samples were also graded with respect to inflammation on a scale of 0 to 10, 10 representing tissue with the most recognized indicators of inflammation.

Figure 8. plots the samples assessed with respect to both inflammation score and the clinical HO grade that was assigned to the site from which the samples were obtained. The inflammation score was derived from two reviewers at Cleveland Clinic and the HO grade, (0-2) was defined for each site by reviewers from NMRC and WRNMMC.

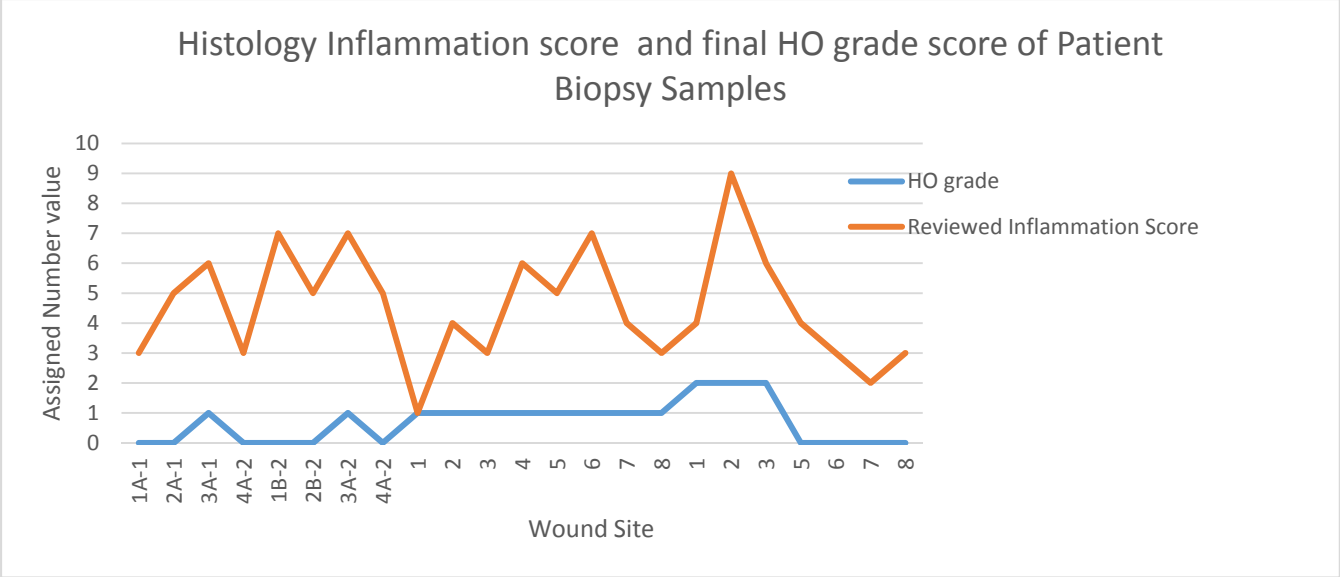

Figure 8. HO grade value 0-2, Inflammation score 0-10. H&E stained biopsy samples from three patients.

These data demonstrate no significant correlation between the inflammation score and the HO grade. The range of inflammation scores in each graft of HO is summarized as follows: Grade 0 = 2-5; Grade 1 = 1 -7; and Grade 2 = 4 – 9.

Figure 9. summarizes the relative tissue composition of the same samples with respect to muscle, fat and fibrosis. Table 4. , below, provides a nomenclature guide for patient would site samples stained with H&E and for Hyaluronan.

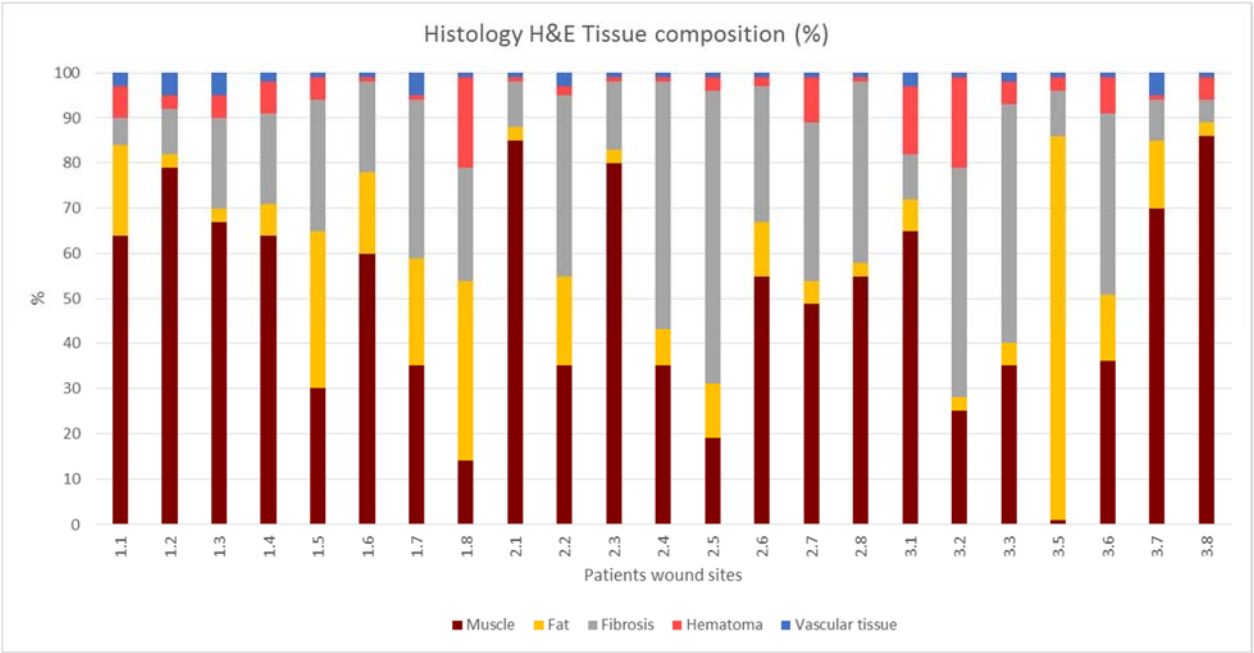

Figure 9. Summary of relative tissue composition for all patient wound sites.

Table 4.

Reference Table for Histology Labeling Nomenclature Linking Patient/Side/Site/Time Point of Debridement																								
Patient	1	1	1	1	1	1	1	1	2	2	2	2	2	2	2	2	3	3	3	3	3	3	3	3
Wound Site	1	2	3	4	1	2	3	4	1	2	3	4	5	6	7	8	1	2	3	4	5	6	7	8
Sample site change					*	*																		
Debridement (week)	1	1	1	1	2	2	2	2	1	1	1	1	1	1	1	1	1	1	1	1	1	1	1	1
NMRC Ref #	1A-1	2A-1	3A-1	4A-1	1B-2	2B-2	3A-2	4A-2	1	2	3	4	5	6	7	8	1	2	3	4	5	6	7	8
CC Histology Ref #	1.1	1.2	1.3	1.4	1.5	1.6	1.7	1.8	2.1	2.2	2.3	2.4	2.5	2.6	2.7	2.8	3.1	3.2	3.3	3.4	3.5	3.6	3.7	3.8

Hyaluronan (HA) Staining and Distribution:

HA is a simple glycosaminoglycan with many complex roles in tissue morphogenesis and inflammation. The role of HA in skeletal biology has been described (1). Both osteoblasts and osteoclasts synthesize HA in bone (2), where HA may be a regulator of mineralization (3). HA is a major component in the many steps of wound healing(4). HA can be free or exist bound to HA binding proteins in extracellular matrix.

Patient biopsy samples present a glimpse of a dynamic process of wound healing. Wound healing involves injured tissue, blood, extracellular matrix, cytokines, and signaling pathways and the wounded warrior presents wounds that are even much more complex due to other tissue injuries and loss. In adults, at the site of wound injury, HA levels increase rapidly and by three days after injury, begin to decrease, (5-6). We postulated that differenes in the intensity and distribution in the HA synthesis response early (6-8 days) after injury may contribute to or mark regions where HO formation as imminent.

Paraffin sections of biopsy samples presented here were stained according to the established protocol of the Glycobiology Core (CC), version 1.1. This protocol presents a method for probing tissues/cells with biotinylated HABP for fluorescent microscopy. Presented below are images of Hyaluronan (HA) stained biopsy samples for patient 01, wound sites 1 through 4, HA stain=green, DAPI nuclei=blue, 20x. HA controls are negative for HA stain pattern. (Figure 10.)

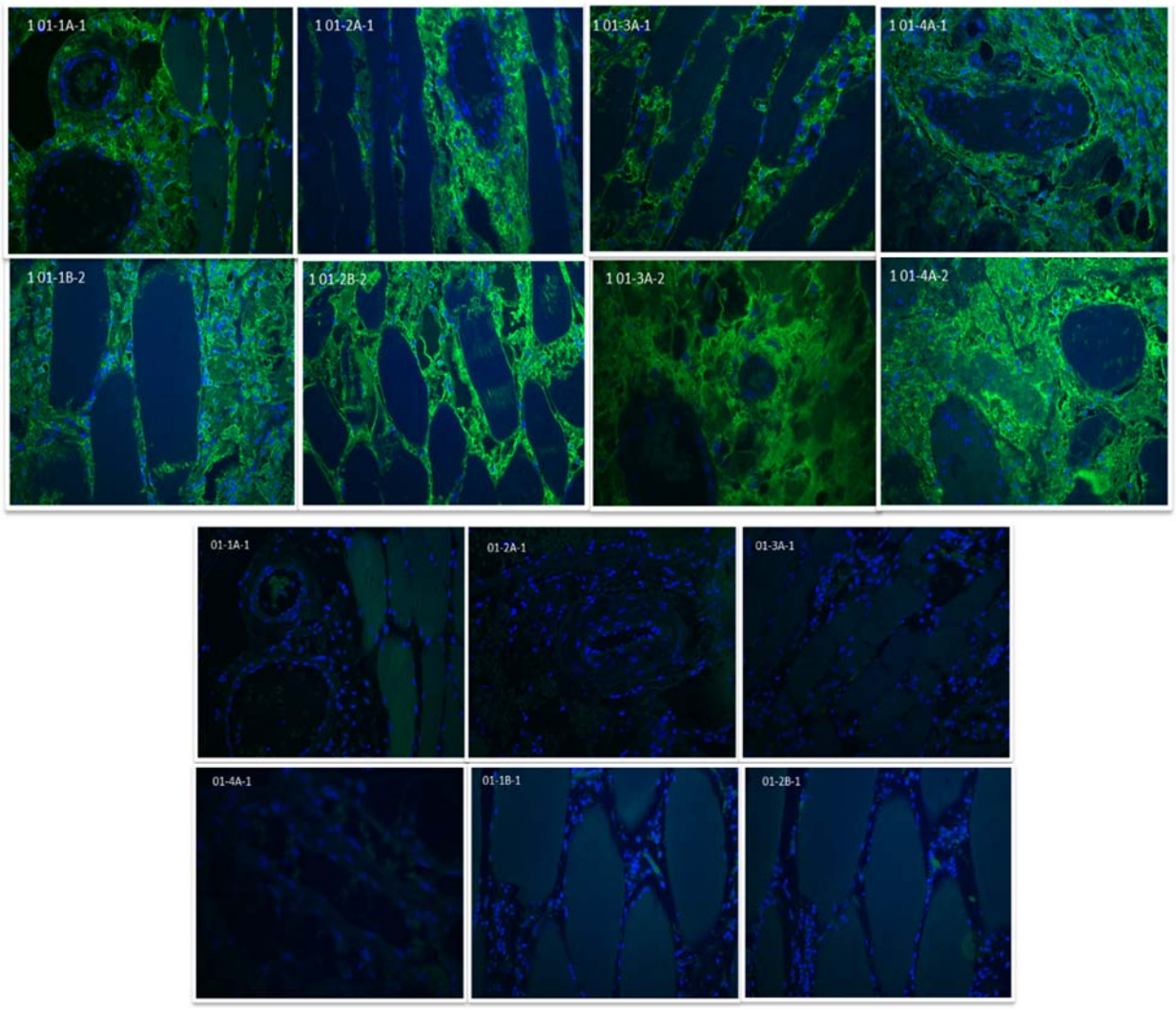

Figure 10. HA Staining – Representative Images (Top 8 panels). HA was present in all biopsy samples. Extracellular HA localized in all areas of tissue injury and inflammation. **HA stain controls** (Bottom six panels) – No binding peptide

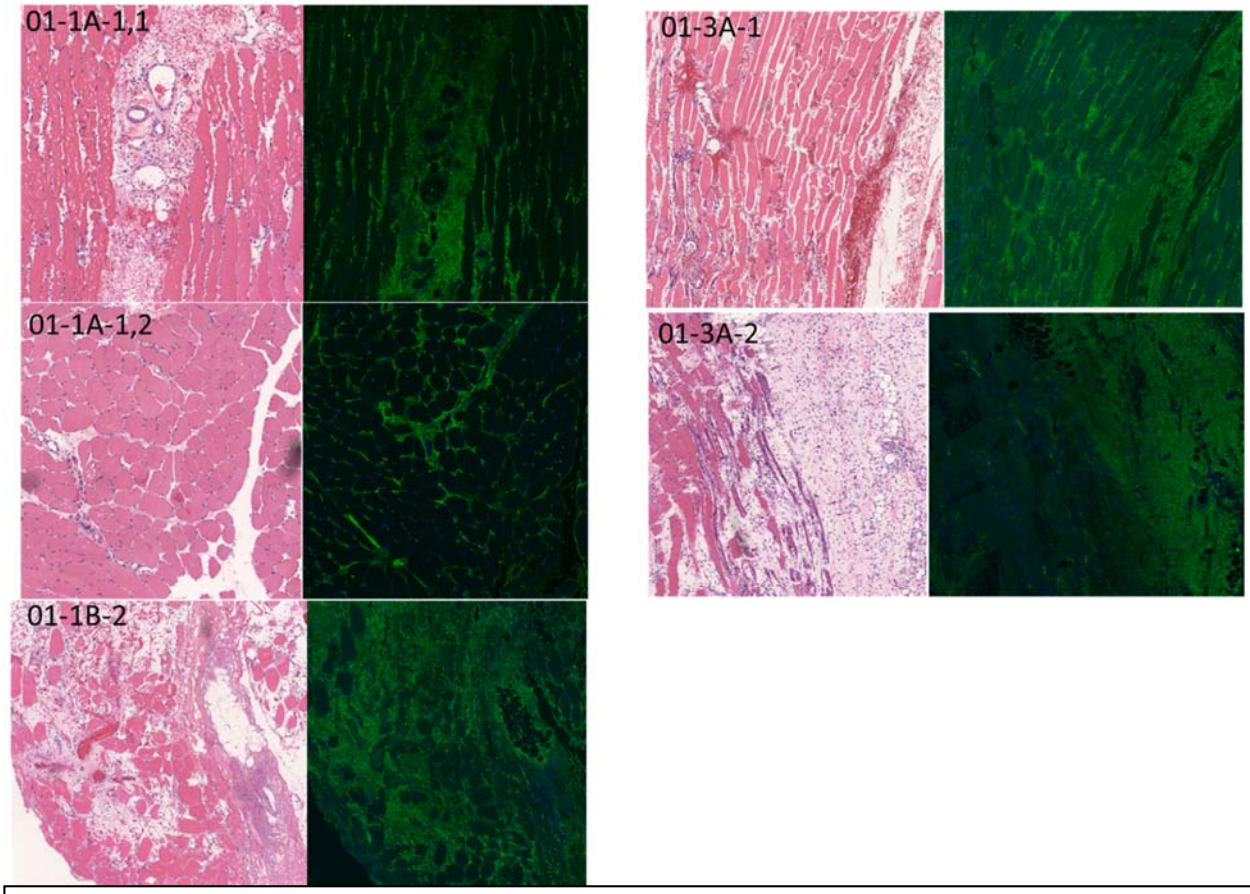

Figure 11. HA Staining – With Corresponding H & E Images

Patient 01 sites 1 (HO+) and 3 (HO-) are shown. Healthy muscle was relatively devoid of HA staining. However HA was found in areas of muscle edema and fibrosis. No differences in HA staining pattern were noted.(Figure 11.).

1.) Bastow,ER, Byers,S.,Golub, S.B.,Clarkin, C.E., Pitsillides, A.A., Fosang, A.J., 2008, Hyaluronan synthesis and degradation in cartilage and bone. Cell. Mole. Life Sci 65(2008) 395-413.

2.) Midura, R.J., X. Su, Morcuende, J.A., Tammi, M., Tammi,R., Parathyroid Hormone rapidly stimulates hyaluronan synthesis by periosteal osteoblasts in the tibial diaphysis of the growing rat. J.Biol. Chem. 278, 51462-51468

3.) Boskey, A.L., and Dick, B.L. (1991), Hyaluronan interactions with hydroxyapatite no not alter in vitro hydroxyapatite crystal proliferation and growth. Matrix 11, 442-446.

4.) Aya, K.L., Stern, R., Hyaluronan in wound healing: rediscovering a major player, Wound Repair and Regeneration, vol. 22, :5, 579-593

5.) Dunphy, JE , Wound Healing, *Surg Clin North Am*1978; **58**: 907–916

6.) Dunphy JE, Udupa KN Chemical and histochemical sequences in the normal healing of wounds. *N Engl J Med*1955*;* **253***:* 847–851.

Specific Aim 2: Develop a predictive model based on a minimum set of clinical variables collected in Aim 1, that will provide clinically useful prediction of where and in whom HO will form.

As discussed previously with the Sponsor and Program Manager, the number of wounded subjects appropriate for enrollment has been far lower than predicted. This is due to the sharp and fortunate decrease in the incidence of traumatic blast-related lower extremity amputees, following the submission and funding of this proposal.

This limited data set was not sufficient to conduct multiplexed measurements with dynamic predictive computational modeling methods.

Specific Aim 3: Identify one or more potential local or topical therapeutic agents that effectively inhibit colony formation, proliferation, differentiation and/or survival of CTP-Os in vitro that could be tested in a subsequent clinical trial.

The effects of Glucose, sodium heparin, and local osmolarity were the first potential therapeutic conditions that were assessed.

Glucose was particularly relevant because it has low risk of systemic toxicity and can be administered intravenously, intra-arterial, topically or via extravasation into extracellular matrix (clysis). Glucose has a low regulatory barrier. Moreover, topical application of high glucose preparations (e.g. honey) have been used historically as a topical wound healing agent without known toxicity.

Heparin is a widely available medication that is used IV for inhibition of coagulation and the prevention of blood clots. Similarly, osmolarity is an important physiological variable that can be clinically difficult to separate from glucose, but which can vary significantly in period following trauma due to changes in ADH secretion following trauma, as well as fluid resuscitation.

Several lines of clinical and laboratory investigation suggest that elevated levels of glucose may have effects on bone formation. Diabetes has been associated with delayed fracture repair, accelerated age-related bone loss, and an increased risk of osteoporosis. Diabetes has also been associated with accumulation of adipocytes in the marrow cavity (fatty conversion of bone marrow), at the expense of bone and hematopoietic tissues. The possible mechanism for glucose effects on cells in culture and in vivo has been extensively studied, but its effects on osteogenesis and particularly the effect of glucose on the proliferation of multipotent native connective tissue progenitors cells (CTPs) and the relative tendency of CTPs to choose an osteogenic fate (bone formation) versus an adipocytic fate (fat formation) is not well understood.

We framed a series of hypotheses related to the effects of high glucose, heparin and osmolarity on human CTP, specifically that these conditions will (alone or in combination):

1. decrease colony forming efficiency, reduce proliferation rate, reduce the number of proliferation cycles before CTPs differentiate, and divert osteogenic cell fate to adipogenic differentiation;
2. induce autophagy-like response in primary human bone-derived CTPs; and
3. heparin will modulate the effects of high glucose culture condition in CTPs.

We designed studies to:

(1) Characterize the effect of high glucose culture conditions on colony forming efficiency, proliferation, and osteogenic differentiation of primary human bone-derived CTPs.
(2) Characterize the effect of high glucose culture condition on the prevalence of autophagy in vitro, (i.e. autophagy-like response in primary human bone-derived CTPs).
(3) Characterize the effect of heparin or heparin-like molecules and their potential to modulate the effects of high glucose culture condition on primary human bone-derived CTPs.

Methods

Human Tissue Samples

Cancellous bone tissue samples, from the proximal femur, were obtained from 7 non-diabetic patients, 4 males and 3 females (mean age: 59 ± 4; range: 48-72). These patients were undergoing elective total hip arthroplasty (THA) procedures at the Cleveland Clinic. Patient tissue samples were collected through an IRB approved protocol and with appropriate consent. All samples were de-identified with respect to personal health information. The overall study design is presented in Figure 12.

Figure 12. Experimental Design to Assess Effect of Glucose Concentration on Human CTPs in Primary Culture in vitro. After isolation dells isolated from the B-TS fraction are placed into culture under six different media conditions controlling for the effect of glucose concentration, osmolarity and the presence or absence of sodium heparin. (*) indicates analysis that was performed using only culture conditions 1-3.

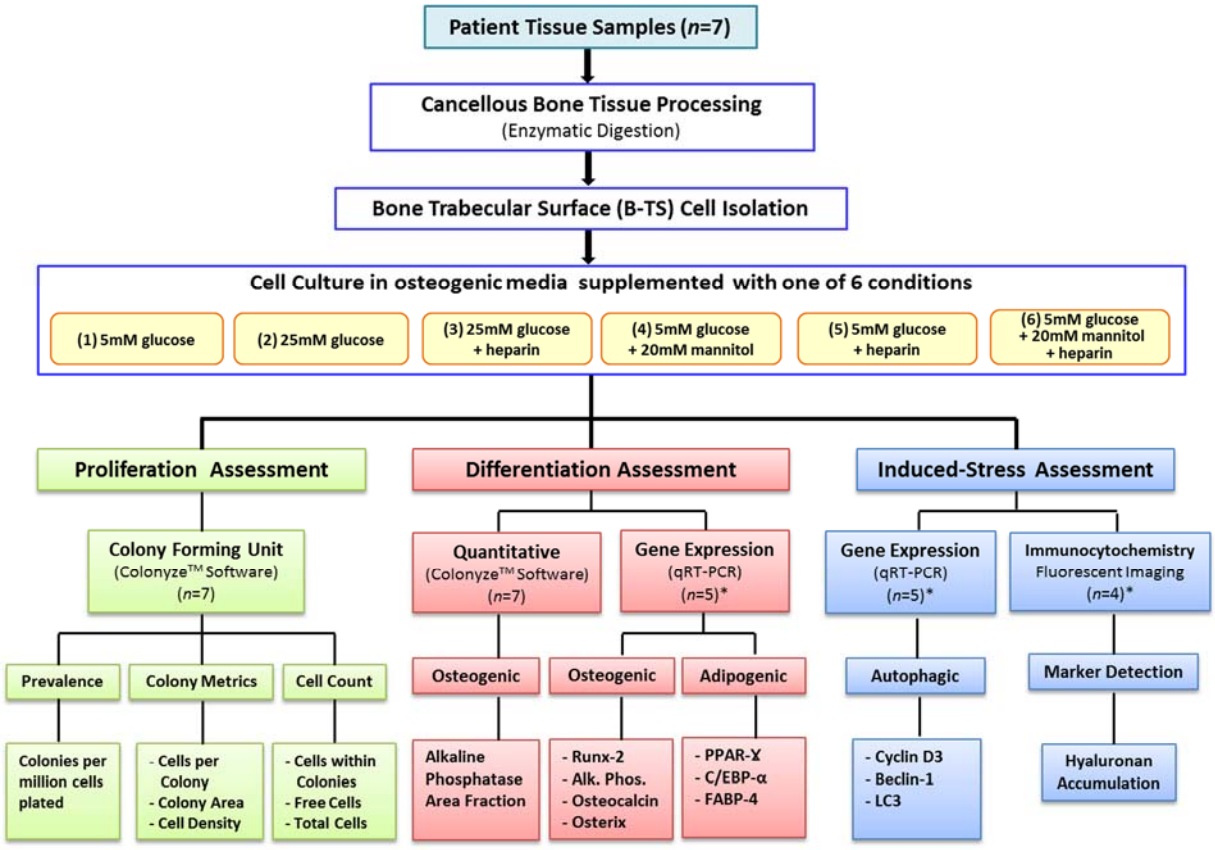

Processing

Cancellous bone tissues were minced into small pieces (1-2 mm^3) with a sharp osteotome. The minced pieces were processed, and the non-adherent cells were removed by mechanical dissociation. This fraction of cells is referred to as the "Marrow Space" (MS) fraction. It contains hematopoietic cells and populations of cells that are not tightly adherent to the trabecular surface. The MS fraction is discarded. Cells that remained adherent to the trabecular surface were then dissociated by enzymatic digestion with 111U/mL collagenase type I/24U/mL dispase (Worthington Biochemical, NJ, USA) for 90 minutes at 37°C. This fraction of cells was used in this study, and defined as the "Trabecular Surface" (TS) cell fraction. The TS population has previously been compared to the MS population and is found to contain a higher prevalence of CTP and CTPs with greater osteogenic potential. Moreover, a mean of 70% of all CTPs in human cancellous bone are present in the "TS" fraction. Cells were filtered through a 70 µm nylon cell strainer (Corning, NY, USA) to separate tissue debris and prepare single cell

suspension. Cells were centrifuged and the pellet suspended in media containing; αMEM, FBS 10% (Atlanta Biologicals, GA, USA), and 1U/mL penicillin/0.1 mg/mL streptomycin (Sigma, MO, USA). The number of cells was counted using a hemocytometer.

Cell Culture

The TS cells were resuspended in osteogenic media containing; αMEM, 10% FBS, 10^{-8} M dexamethasone (D-1756, Sigma, MO, USA), 50 μg/mL ascorbate (Sigma, St. Louis, MO, USA), and 1U/mL penicillin/0.1 mg/mL streptomycin. Osteogenic media used were prepared supplemented with one of 6 culture conditions as listed in Table 5. Cells were plated at 2.5 X 10^5 nucleated cells per chamber (4.2 cm^2) in 2 well Lab-Tek™ chamber slides (Thermofisher Scientific, Nunc, NY, USA). Cultures were incubated at 37°C in a humidified atmosphere of 5% CO_2 in 3% oxygen using Oxycycler™ chambers (Biospherix, Redfield, NY, USA). Oxygen tension was set to 3% O_2, because this represents normal physiological oxygen tension in the trabecular surface microenvironment and has previously been found to optimize colony forming efficiency in human bone derived CTPs. Based on previous evaluation, we found that, cultures of CTPs at low oxygen tension resulted in an increase in proliferation and higher colony forming efficiency compared with cultures incubated at 20% O_2.[1,2]Non-adherent cells were removed 48 hours after initial plating. Medium was changed every 2 days.

Table 5. Culture conditions and the purpose per each condition used, for the assessment of the effect of high glucose (with and without heparin) on bone-derived trabecular surface primary cells.

Culture Condition	Concentration	Purpose
(1) Normal glucose	5 mM glucose	Physiological glucose level.
(2) High glucose	25 mM glucose	Hyperglycemia level.
(3) High glucose + heparin	25 mM glucose + 2 μg/mL heparin	Proposed-rescue of high glucose effect
(4) Normal glucose + mannitol	5 mM glucose + 20 mM mannitol	Osmolarity control.
(5) Normal glucose + heparin	5 mM glucose + 2 μg/mL heparin	Test the effect of heparin alone
(6) Normal glucose + mannitol + heparin	5 mM glucose + 20 mM mannitol + 2 μg/mL heparin	Osmolarity control with heparin.

Characterization of the effect of high glucose (with and without heparin) culture conditions on bone-derived CTPs

(a) Colony Forming Efficiency, Colony Metric, and Cell Count

Cells were cultured in osteogenic media with each of the 6 culture conditions Table (2) in chamber slides for 6 days. Cells were washed with 1X PBS and fixed with 1:1 acetone-methanol (Fisher, Pittsburgh, PA, USA) for 10 min then air dried. To localize cells and colonies, nuclei were stained with mounting medium containing DAPI (4', 6-diamidino-2-phenylindole) (H1200, Vector Laboratories, CA, USA). Stained cultures were stored at room temperature, in the dark, until image acquisition. Fluorescent images of nuclei, in the entire culture area, were captured and processed as described by Powell, et al.[3]. To determine the proliferative potential of primary TS cells, an established colony forming unit (CFU) assay utilizing Colonyze™ image analysis software was used.[37,38,40] for quantitative characterization of each colony. A colony at day 6 was defined as a group of 8 or more cells, based on proximity suggesting a common founding cell (i.e. CTP). To compare the *in vitro* performance of the progeny of founding CTP, we measured and compared CTPs under the culture conditions with respect to: (1) colony forming efficiency (CFE) by measuring observed prevalence of CTPs (oP_{CTP}) (number of colonies per million nucleated cells plated);[4] (2) colony metrics: (a) cells per colony (metric of proliferation)

[38,40] (b) colony area (mm^2, measured by nuclei distance mapping), and (c) colony density (cells per mm^2, metric of cell migration); and (3) cell counts (within colonies, cells not included in colonies (free cells), and total cells). These provided metrics of relative proliferation.

(b) Osteogenic Differentiation Potential

Cells were cultured in osteogenic media with each of the 6 culture conditions, on chamber slides for 6 days. Cells were washed with 1X PBS and fixed with 1:1 acetone-methanol for 10 min then air dried. To recognize cells and colonies, nuclei were stained with DAPI. Cells were stained for alkaline phosphatase (AP) detection using Vector-Red® AP substrate kit (SK-5100, Vector Laboratories, CA, USA). AP staining was used as a marker of early osteoblastic differentiation.[3,5,6,7] Colonyze™ image analysis software was used [1,2,3] for quantitative characterization of each colony based on area fraction of AP expression (A_{AP}). For each colony we measured; (1) A_{AP} per total colony area (a measure of relative differentiation among colonies with respect to AP expression; (2) A_{AP} per total cells in each colony (a measure of relative differentiation among the cells in each colony with respect to AP expression.

(c) Gene Expression Analysis using qRT-PCR

Quantitative Real-Time PCR (qRT-PCR) was used to detect the expression of related marker genes for: (1) osteogenic differentiation (Runx-2, AP, osteocalcin, and oxterix); (2) adipogenic differentiation (C/EBPα, FABP-4, and PPAR-Ɣ); and (3) Autophagic-response related markers (Cyclin D3, Beclin-1, and LC3).

Cells were cultured in 6 well plates (Corning, ME, USA) in osteogenic differentiation media supplemented with each of 3 culture conditions (5 mM glucose, 25 mM glucose, and 25 mM glucose + 25 µg/mL heparin). Cultures were incubated until they reached 80% - 90% confluence, approximately 10-14 days from initial plating. Adherent cells were washed with 1X PBS and harvested using 0.5% trypsin/1mM EDTA (Sigma-Aldrich, St. Louis, MO, USA). Cell pellets were stored in -80°C until analysis. Cell pellets were homogenized in lysis buffer and total RNA was extracted using MicroElute® Total RNA Kit (Omega bio-tek, GA, USA).

Total RNA concentration was determined using Nano-Drop® spectrophotometer (ND-1000, NanoDrop Technologies, DE, USA). For cDNA synthesis, 1 µg of total RNA per 20 µl reverse transcription reaction was used. Reverse transcription reaction was performed using qScript™ cDNA SuperMix (Quanta Biosciences, MD, USA). cDNA was amplified using primers for osteogenic, adipogenic, and autophagic markers as well as for housekeeping gene (Table 6). The amplification reaction was performed using PerfeCTa® SYBR® Green SuperMix (Quanta Biosciences, MD, USA) with Real-Time System (CFX96™, BIO-RAD, CA, USA). The expression of each gene was analyzed in triplicate.

For each gene the expression level was normalized to glyceraldehyde-3-phosphate dehydrogenase (GAPDH) gene, which was used as an internal control. Fold change was measured by the $2^{-\Delta\Delta CT}$ method. The PCR product per each amplified gene was verified using agarose gel electrophoresis.

Table 6**.** Sequences of primers used in quantitative real-time polymerase chain reaction (qRT-PCR).

Gene	Gene Bank ID	Primer Sequence
Osteogenic Differentiation Markers		
RUNX-2 **Runt-related transcription factor 2 or (CBFA1)**	NM_004348	Right-CCTAAATCACTGAGGCGGTC Left-CAGTAGATGGACCTCGGGAA
ALP **Alkaline Phosphatase**	NM_000478	Right-GCTGGCAGTGGTCAGATGTT Left-CTATCCTGGCTCCGTGCTC
Osteocalcin **Bone gamma-carboxyglutamate protein, BGLAP**	NM_l99173	Right-CCTCCTGCTTGGACACAAAG Left-TGAGAGCCCTCACACTCCTC
Osterix **SP7 transcription factor, SP7**	NM_152860	Right-GGGACTGGAGCCATAGTGAA Left-CTCAGCTCTCTCCATCTGCC
Adipogenic Differentiation Markers		

C/EBPα **CCAAT/Enhancer Binding Protein**	NM_004364	Right-TTCACATTGCACAAGGCACT Left-ACGATCAGTCCATCCCAGAG
FABP4 **Fatty Acid Binding Protein 4 or (aP2)**	NM_001442	Right-ACTTTCCTGGTGGCAAAGC Left-GCAGCTTCCTTCTCACCTTG
PPARɣ2 **Peroxisome proliferator-activated receptor gamma**	NM_015869	Right-TTACGGAGAGATCCACGGAG Left-CCTATTGACCCAGAAAGCGA
Autophagic Markers		
Cyclin D3	NM_001760	Right-GAATGAAGGCCAGGAAATCA Left-CCCTGACCATCGAAAAACTG
Beclin-1	NM_003766	Right-CCTGGCGAGGAGTTTCAATA Left-TGTCACCATCCAGGAACTCA
LC3 **Microtubule-associated proteins 1A/1B light chain 3A**	NM_181509	Right-GCTGTACCTCCTTACAGCGG Left-TGACTGACCCTCCACCTCA
Housekeeping Gene		
GAPDH **Glyceraldehydes-3-phosphate-dehydrogenase**	NM_002046	Right-TTGAGGTCAATGAAGGGGTC Left-GAAGGTGAAGGTCGGAGTCA

(d) Immunocytochemistry for detection of HA accumulation.
Cells were cultured in osteogenic media with each of 3 culture conditions (normal glucose, high glucose, and high glucose + heparin), in chamber slides for 6 days. Cells were fixed with 4% paraformaldehyde (EMS, PA, USA) for 15 minutes. After three washes with 1X PBS, cells were blocked with 0.1% BSA (BP1600-100, Fisher Scientific, NJ, USA) for 30 minutes. For intracellular detection of HA, cells were permeabilized with Triton X-100 (LabChem Inc., PA, USA) for 10 minutes at room temperature then blocked with 0.1% BSA. To detect HA accumulation, cells were incubated with biotinylated hyaluronic acid binding protein (HABP) (EMD Millipore, MA, USA) over night at 4°C. After three washes with 1X PBS, cells were incubated with Streptavidin-Alexa Fluor-488 conjugated antibodies (Molecular Probes, S-11223, MA, USA) for 60 minutes at room temperature. Another set of slides containing fixed cells were incubated with Streptavidin-Alexa Fluor-488 conjugated antibodies (secondary antibodies only). Stained cells were covered with mounting medium containing DAPI (4', 6-diamidino-2-phenylindole) (H1200, Vector Laboratories, CA, USA). Fluorescent images were captured with fluorescent (Leica, IL, USA) and confocal microscopes (Leica Microsystems, GmbH, Wetzlar, Germany). Image J software was used to create the merged colored images.

Data Analysis
Data outcomes from Colonyze^{TM} CFU-assay, quantitative osteogenic differentiation, and gene expression analysis are presented as means ± standard error of the mean (SEM). Two-tailed *t*-test was used to compare groups for statistical significant differences. Differences were considered significant at $P \leq 0.05$.

Results

Effect of glucose, heparin and hyperosmolarity culture conditions on colony forming efficiency, colony metric, and cell count

We assessed the effect of high glucose (with and without heparin) culture conditions on CFU, colony metrics, and cell counts at day six of culture of CTPs. We determined the oP$_{CTPS}$, colony metrics (cells per colony, colony area, and cell density), and cell counts (cells within colonies, free cells, and total cells) using Colonyze ^{TM} CFU assay. Data outcomes are listed in (Table 7).

Table 7**.** Effects of high glucose (with and without heparin) culture conditions on colony forming efficiency, colony metrics, and cell counts of bone-derived CTPs, at day 6 of culture. Parameters are data outcomes from colony forming unit-assay using Colonyze^{TM} software. Data are presented as ratios normalized to 25 mM glucose condition. (*) indicates significant difference compared with normal glucose culture condition, and (#) indicates significant difference compared with high glucose culture condition. Data are expressed as Mean ± Standard Error.

Parameter	5 mM Glucose	25 mM Glucose	25 mM Glucose + Heparin	5 mM Glucose + 20 mM Mannitol	5 mM Glucose + Heparin	5 mM Glucose + 20 mM Mannitol + Heparin
Observed Prevalence (oP_{CTP})	1.27 ± 0.16	1.00 ± 0.00	0.70 ± 0.05* #	0.87 ± 0.12	1.11 ± 0.33	1.19 ± 0.31
Cells/Colony	1.18 ± 0.12	1.00 ± 0.00	0.93 ± 0.11	1.12 ± 0.07	0.85 ± 0.09	0.94 ± 0.11
Colony Area	1.16 ± 0.15	1.00 ± 0.00	0.87 ± 0.12	1.15 ± 0.10	0.81 ± 0.11	0.86 ± 0.14
Cell Density	1.02 ± 0.03	1.00 ± 0.00	1.05 ± 0.03	0.99 ± 0.02	0.99 ± 0.03	1.05 ± 0.04
Cells within Colonies	1.43 ± 0.19	1.00 ± 0.00	0.66 ± 0.07* #	0.94 ± 0.13	1.10 ± 0.36	1.12 ± 0.29
Free Cells	1.06 ± 0.05	1.00 ± 0.00	0.90 ± 0.02* #	0.95 ± 0.05	1.04 ± 0.08	1.10 ± 0.13
Total Cells	1.22 ± 0.10	1.00 ± 0.00	0.80 ± 0.03* #	0.93 ± 0.06	1.05 ± 0.17	1.10 ± 0.17

Table 7. Summary Colony Forming Efficiency and Colony Metrics Data. All Data normalized to 25 mM glucose conditions (n=7)

Overall these data demonstrate substantial individual variation. The data suggest that significant glucose effects are present. However, they also suggest that a larger sample size to fully elucidate the effects of glucose, osmolarity and heparin. This accumulation of further samples in ongoing.

Colony Forming Efficiency

- High gucose conditions were associated with lower CFE. Mean ratio of the oP_{CTP} for 5 mM vs 25mM glucose was 1.27 ± 0.16). However, this was not statistically significant in this small sample size (P = 0.18), likely due to beta error.
- Heparin may have a negative effect on CFE. Contrary to predictions from prior reports, heparin did NOT rescue high glucose effect. Instead, the mean ratio of the oP_{CTP} in 25 mM glucose w/ heparin culture vs w/o heparin was (0.70 ± 0.05). This difference was statistically significant (P = 0.002) and even higher than 5 mM glucose (P = 0.019).
- Osmolarity or Mannitol may also have an effect. The oP_{CTP} in the osmolarity control group containing 20 mM mannitol, was slightly decreased compared with 5 mM glucose culture condition, but the difference was not significant. An alternative to mannitol should be considered in the future studies as an osmolarity control.

Proliferation of CTP Progeny In Vitro

- Low glucose and mannitol has no effect on proliferation. Mean ratio of cells per colony in 5 mM vs 25 mM glucose group was 1.18 ± 0.12 (P = 0.22). Similarly, when heparin was present, the ratio of 5 mM and 25 mM glucose were similar. The mean ratio of 5 mM glucose + 20 mM mannitol was (1.12 ± 0.07).
- Heparin again suggested a negative effect on proliferation manifest by smaller colony size in both the 5 nM and the 25 nM glucose groups.

Differentiation – Colony Area

- Mean ratio of colony area in the 5 mM vs 25 mM glucose culture condition was 1.16 ± 0.15, P = 0.37.
- Heparin again trended negative, with a mean ratio of colony area in the 25 mM glucose w/ vs w/o heparin of 0.87 ± 0.12, P = 0.38.
- The mean ratio in the 5 mM glucose + 20 mM mannitol was (1.15 ± 0.10) similar to the ratio in 5 mM glucose.

Differentiation – Colony Density

- Mean cell density, in all of the culture conditions, was similar across all conditions.

Adherenct Cells Outside of Colonies

- Glucose concentration did not affect free cell count in the 5 vs 25 mM glucose culture condition were similar (ratio 1.06 ± 0.05).
- Heparin had an impact on the number of non-colony cells. The ratio of free cells in the 25 mM glucose w/ vs w/o heparin was (0.90 ± 0.02) (P = 0.003). This was also significantly reduced in the 5 mM glucose condition (P = 0.034).
- Osmolarity alone did not have an effect.

Effect of glucose, heparin and hyperosmolarity culture conditions on differentiation (alkaline phosphatase area fraction (A_{AP}) per cell area)

We evaluated the effect of glucose, heparin and osmolarity osteogenic differentiation potential bone-derived CTPs using the expression of alkaline phosphatase as a marker. Using Colonyze™ software, we measured A_{AP} per cell area, a measure of relative differentiation among the cells in each colony with respect to AP expression. Data outcomes are presented as mean ratios normalized to 25 mM glucose culture condition (Table 8).

Glucose

- The mean ratio of A_{AP} per cell area was slightly higher in 5 vs 25 mM glucose was 1.24 ± 0.11 (P = 0.09), trending to increased AP activity.

Heparin

- Heparin was associated with an increase in AP expression at both 5 and 25 nM Glucose.
- The mean ratio of A_{AP} per cell area in 25 mM glucose w/ vs w/o heparin was 1.79 ± 0.38, but by itself was not significant (P = 0.10).
- The addition of heparin under 5 mM glucose condition with or without mannitol was also associated with increased AP rexpression, tipping the weight of evidence for a heparin effect.

Osmolarity

- Osmolarity did not have an independent effect on AP expression.

These data are presented as bar graphs in Figure 13. A. Raw data demonstrating the variation between individuals is illustrated in Figures 13. B-C. Note that the direction of response also showed marked individual variation, complicating the analysis of direct effects of these individual culture conditions.

SUMMARY: Overall these data are consistent with a possible benefit of the combination of 25 mM glucose and heparin in decreasing CTP colony forming efficiency and proliferation. The combination of heparin and glucose increased AP expression. However, in the setting of smaller colonies, ths finding could suggest that heparin increases the rate of differentiation, cutting short the proliferation of pre-osteogenic cells, which could result in decreases in the amount of new bone formation.

These findings are highly preliminary, however, but both glucose and heparin represent low toxicity agents that are worthy of further evaluation as tools for local suppression of CTP activation and proliferation and subsequent bone formation following blast injury.

Parameter	5 mM Glucose	25 mM Glucose	25 mM Glucose + Heparin	5 mM Glucose + 20 mM Mannitol	5 mM Glucose + Heparin	5 mM Glucose + 20 mM Mannitol + Heparin
A_{AP} per Cell Area	1.24 ± 0.11	1.00 ± 0.00	1.79 ± 0.38	1.03 ± 0.08	1.71 ± 0.35	1.59 ± 0.33

Table 8. Summary AP Data normalized to 25 mM glucose conditions

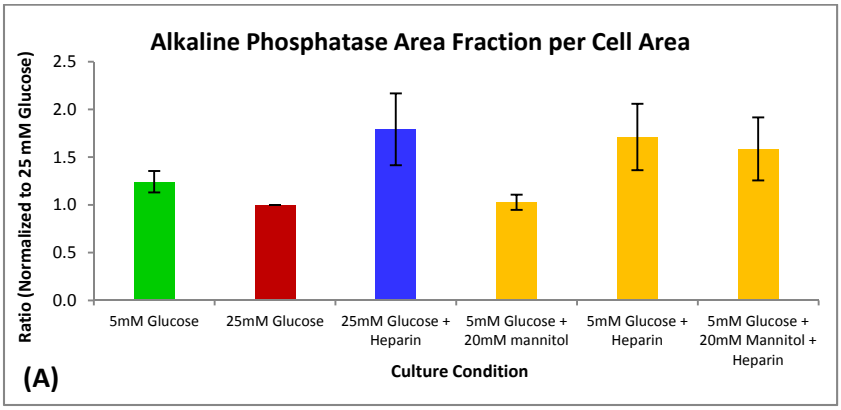

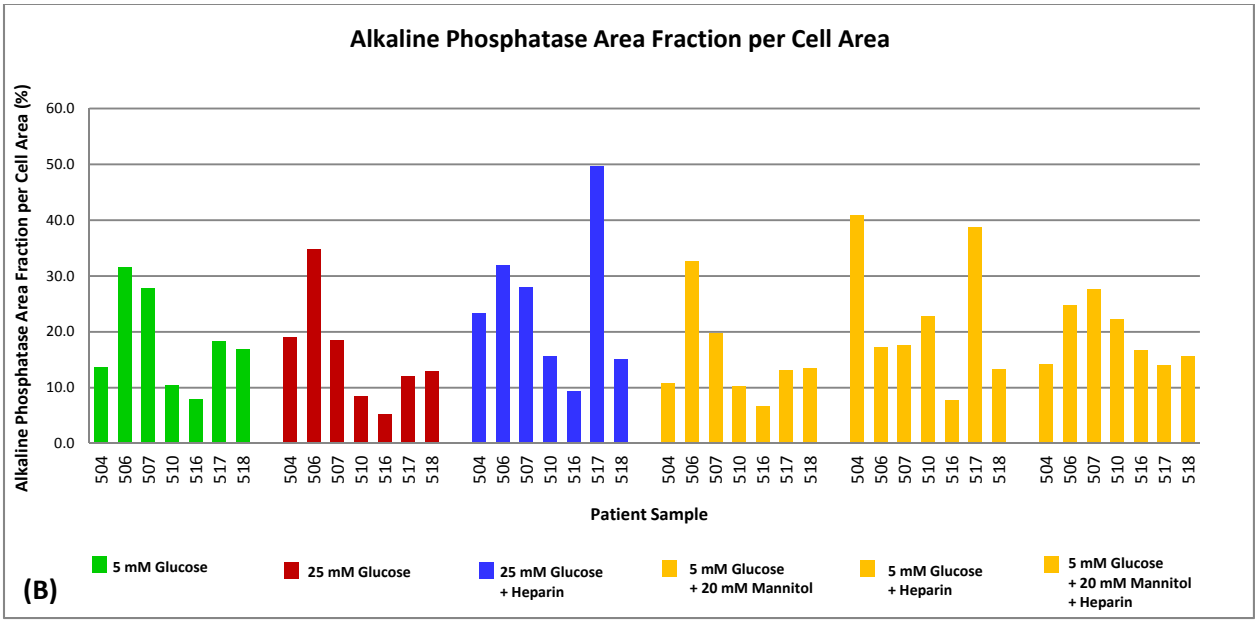

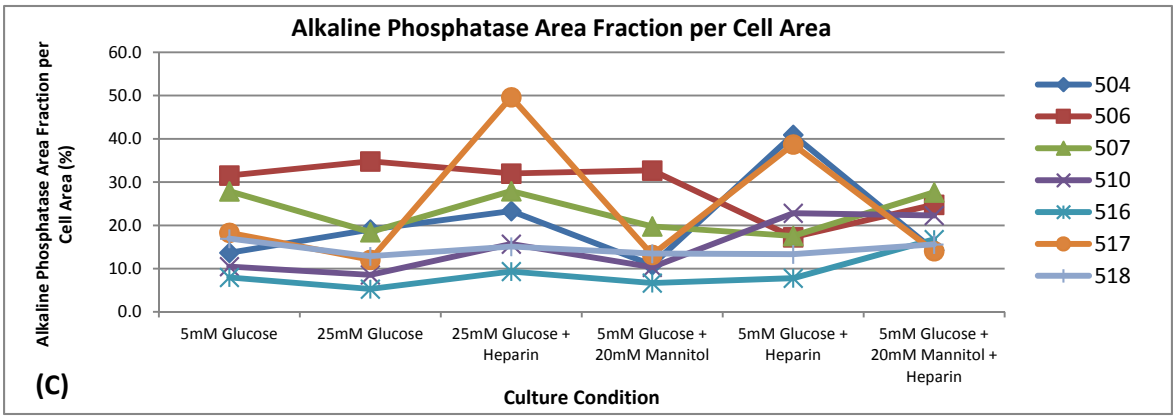

Figure 13. A-C. Summary AP Data normalized to 25 mM glucose conditions: A. Presented as a bag graph with Data are expressed as Mean ± Standard Error, (n = 7). B. Raw data for each individual illustrating the magnitude of variation between subjects. (C) Dot plot represents response of each individual patient sample to each culture condition. Dots are connected by a colored line correspond to each individual patient sample.

Gene Expression Analysis

Glucose, Heparin and Osmolarity Effects on Osteogenic and Adipogenic Differentiation-related Markers

Gene expression was also used to assess the effect of glucose and heparin on osteogenic and adipogenic differention. Using gene expression analysis by qRT-PCR, we determined the fold change in expression of osteogenic (Runx-2, AP, and osteocalcin) and adipogenic (C/EBP-α and FABP-4) differentiation-related markers compared to normal glucose culture condition. These data are summarized in Figure 14 - A through C, below.

We observed that the expression levels of the osteogenic marker (osterix) and the adipogenic marker (PPAR-Ɣ), late markers of bone and fat differentiation were not detectable within the culture time period used in this study. Consistent with the colony analysis data, expression of AP was 1.42 fold higher in 25 mM glucose compared with 5 mM glucose culture condition.

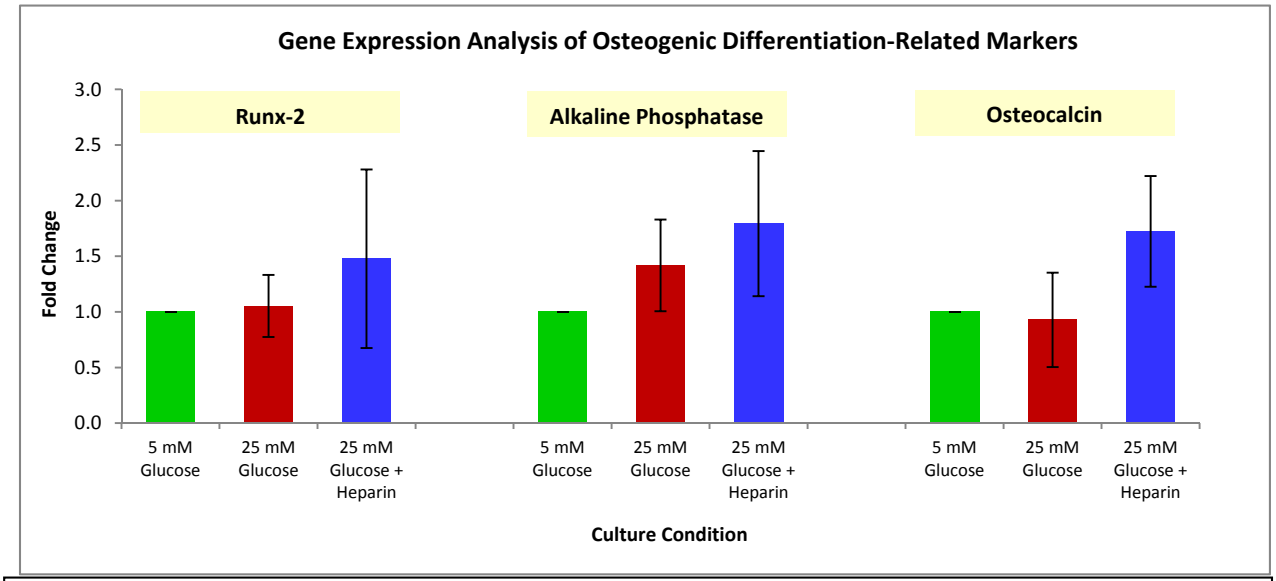

Figure 14 - A. Effect of high glucose (with and without heparin) culture conditions on osteogenic differentiation potential of bone-derived CTPs. Bar graph shows fold change of gene expression, of Runx-2, alkaline phosphatase, and osteocalcin, normalized to 5 mM glucose culture condition. Data are expressed as Mean ± Standard Error, n = 5. CTP: Connective Tissue Progenitor.

Runx-2 and osteocalcin expression was comparable at 5 and 25 mM glucose. However, the mean expression of Runx-2, AP, and osteocalcin were all highest in the setting combining 25 mM glucose + heparin (1.48, 1.79 and 1.72 fold, respectively), however these differences wre not statistically significant.

Mean expression of the adipogenic differentiation marker C/EBP-α was unchanged by glucose or heparin.

Expression of FABP-4 was also increased by 25 mM glucose and heparin, although these 2.15 and 1.56 fold changes were not statistically significant.

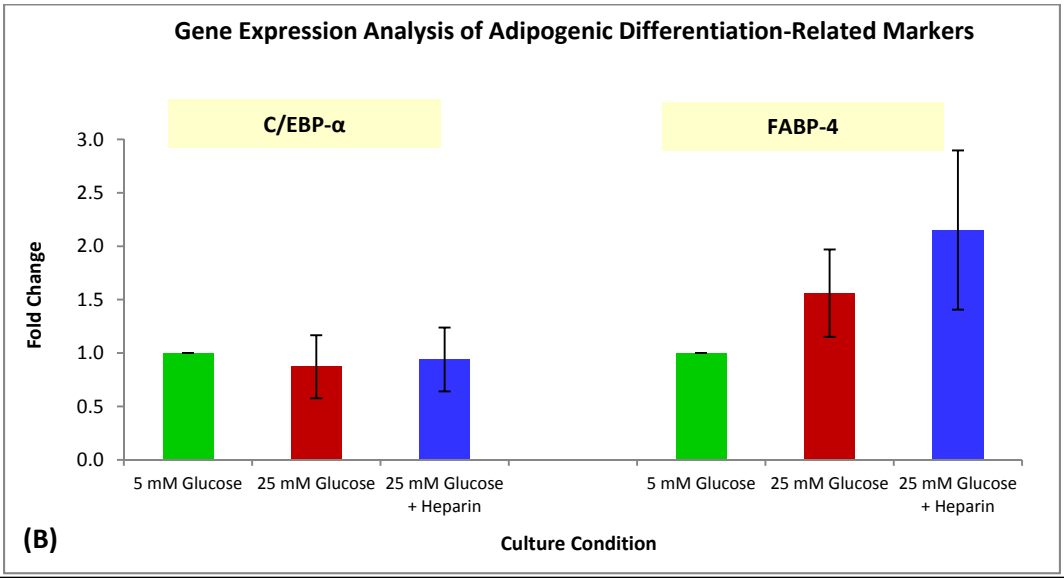

Figure 14 - B. Effect of high glucose (with and without heparin) culture conditions on adipogenic differentiation potential of bone-derived CTPs. Bar graph shows fold change of gene expression, of C/EBP-α and FABP-4, normalized to 5 mM glucose culture condition. Data are expressed as Mean ± Standard Error, n = 5. CTP: Connective Tissue Progenitor

Glucose, Heparin and Osmolarity Effects on Autophagy-like Response-related Markers

The expression of autophagic responses-related markers cyclin D3increasdd under high glucose condition, consistent with a high glucose induced a stress-like response (1.67 and 1.90 fold, respectively), but these changes were not statistically significant.

Expression of Beclin-1 was not changed and the expression levels of LC3 were not detectable within the time period of culture used in this study.

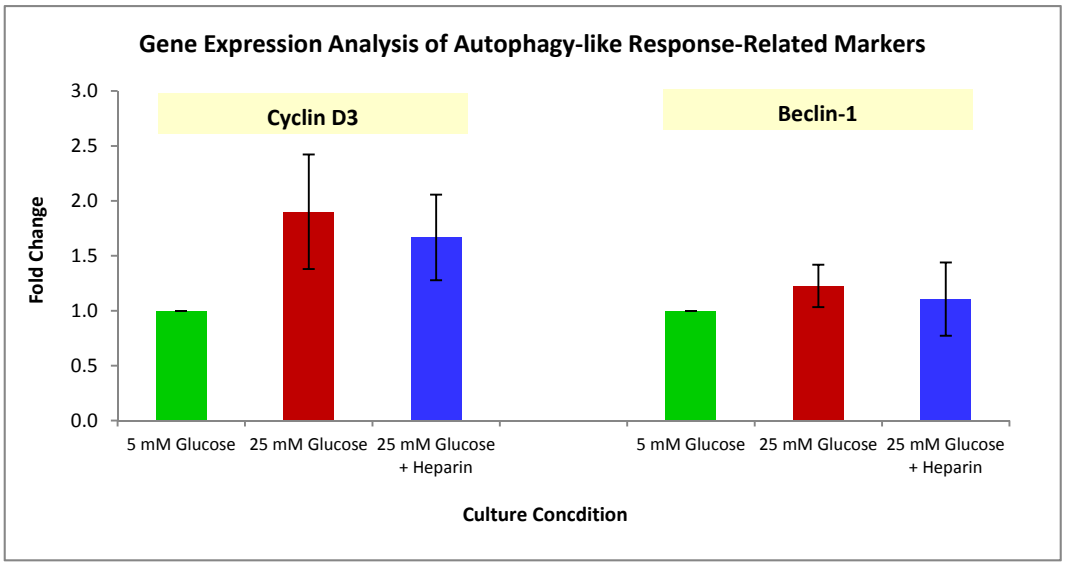

Figure 14 - C. Effect of high glucose (with and without heparin) culture conditions on autophagy-like response related markers of bone-derived CTPs. Bar graph shows fold change of gene expression, of cyclin D3 and beclin-1, normalized to 5 mM glucose culture condition. Data are expressed as Mean ± Standard Error, $n = 5$. CTP: Connective Tissue Progenitor.

Histological Detection and Distribution of HA in CTP progeny In Vitro

We assessed the effect of glucose and heparin on the culture expanded progeny of colony founding CTPs at day 6 of culture.

The pattern of distribution of HA may vary between culture conditions and among cells and colonies in same culture condition of same sample.

We observed a greater accumulation of HA in 25 mM glucose + heparin compared with all the other culture conditions in both permeabelized and non-permeabelized cells (Figure 15.).

We observed that HA presented in a unique pattern surrounding compacted colonies in 5 mM glucose culture condition. HA appeared as dense accumulation with cable-like structures in certain colonies in the 25 mM glucose. HA distribution in 5 mM glucose + heparin and in mannitol culture conditions was similar to 25 mM culture condition but in limited colonies. HA was not detected in cells stained with secondary antibodies only.

Overall, these observations were consistent with a glucose stress response under 25 mM glucose

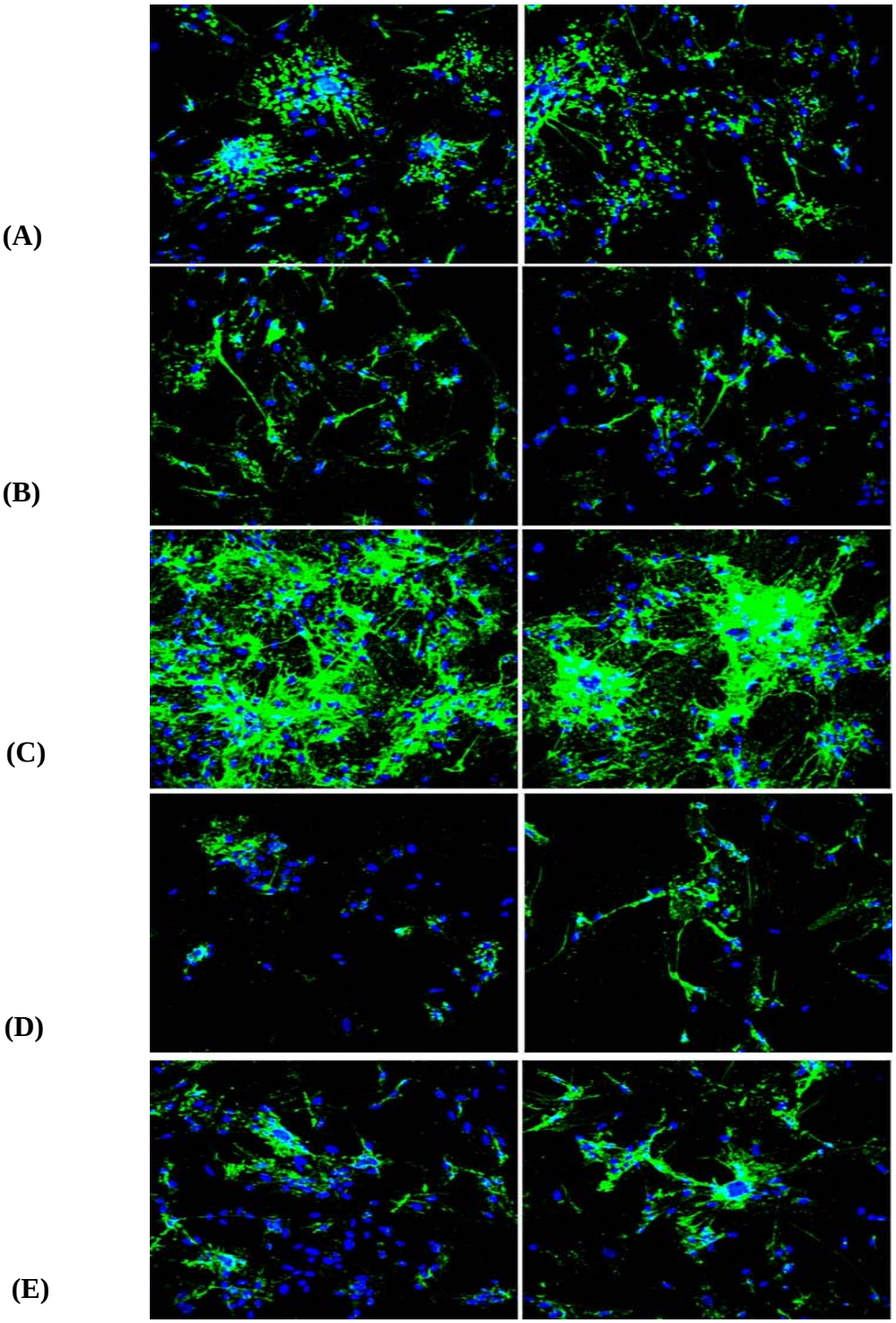

Figure 15. Effect of high glucose (with and without heparin) culture conditions on hyaluronan (HA) accumulation in the bone-derived CTPs at day 6 of culture. Left panel represents images of non-permeabilized cells; and right panel represents images of permeabilized cells (by Triton X-100). (A) Normal glucose (5 mM); HA accumulates around colonies. (B) High glucose (25 mM); HA cable-like appeared extended between cells. (C) High glucose (25 mM) + heparin; extensive HA accumulation appeared. (D) Normal glucose (5 mM) + heparin; relatively low amount of HA accumulation appeared. (E) Normal glucose (5 mM) + mannitol (20 mM); used as osmotic control. Nuclei stained with DAPI (blue); and HA stained with AlexaFluor-488 (green). (Images by Confocal microscope 20X Dry Lens).

Specific Aim 4: Characterize the heterogeneity and evolution of the biological environment in tissue sites in traumatic amputations of the lower extremity in the Rat HO model between week 1 and week 3 following injury using multiple modalities.

Blasts and high-energy projectiles cause the majority of modern war wounds. The physiological insults produced by blast overpressure trauma account for approximately 70% of all combat-related war injuries involving soft tissue, bone, and neurovascular structures. Acute wound failures and subsequent heterotopic ossification (HO) formation are related to multiple complex inter-related systemic and local inflammatory responses to blast-related traumatic injury. In comparison to the civilian trauma setting, trauma-induced HO is vastly more prevalent in the military setting, occurring in approximately 65% of amputations and nearly 62% of limb sparing procedures. We have established and characterized a rat model of trauma-induced HO that incorporates the critical injury patterns commonly seen in human combat casualties specifically a blast injury, comminuted femur fracture, a thigh-crush and a transfemoral amputation through the zone of injury. In this model, radiographic evidence of ectopic bone development is measurable in 100% of injured rats with nominal mortality (< 2%). Treatment strategies to prevent combat-related HO has garnered a greater focus as current prophylaxis strategies used in civilian trauma, such as post-operative administration of non-steroidal anti-inflammatory drugs and external-radiation beam therapy can be contraindicated in patients who sustain systemic combat or blast-related trauma. We postulate the microenvironment that supports ectopic bone development contains a dynamic composite of cells within an inflammatory, osteogenic and angiogenic milieu and scaffold of extracellular matrix, where osteogenic stem/progenitor cells thrive. Our investigative approach has shifted to therapeutic and prevention strategies focused on identifying the origin and targeting progenitor cells towards altering the ectopic bone microenvironment that supports early ectopic bone development and progression. The retinoid signaling is important for chondrocyte maturation and endochondral bone formation. Shimono et al. demonstrated in a mouse genetic model of fibrodysplasia ossificans progressiva (FOP), a rare untreatable genetic disorder of progressive extraskeletal ossification, that the retinoic acid receptor γ (RARγ) agonist Palovarotene effectively inhibits HO formation via suppression of chondrocyte maturation and early cartilage vascularization. In this study, we assessed the capacity of Palovarotene treatment to (1) block trauma-induced ectopic bone formation; (2) suppress local and systemic inflammatory responses; and (3) suppress osteogenic progenitor cell development (proliferation/expansion/differentiation) within the injury site.

Experimental study design

A total of 84 adult male Sprague Dawley rats (450-500 g) were used. Using our established combat-injury model (blast overpressure of 120 ± 7 kPa from a shock tube, comminuted femoral fracture, one minute thigh crush injury and amputation through zone of injury), rats were treated with either 100µl of vehicle control (3% DMSO/corn oil) or Palovarotene (1.0 mg/kg) via oral gavage every other day for 14 days, starting at postoperative day 1 (POD-1). In an initial study arm, surgical sites were monitored longitudinally over 84 days for evidence of wound dehiscence and ectopic bone formation using MicroCT imaging to quantitate total new bone and ectopic bone (non-associated with cortical margins) volume. In a second study arm, serum was collected and assayed (Luminex multianalyte profiling) for various inflammatory mediators from cohorts of rats euthanized at PODs 1, 3, 7, 10, 14, and 21 (n=5 rats /treatment/time point). Next, soft tissue extracellular matrix collagen and mineralization at the distal portion of the residual limb was assessed by Raman Spectroscopy using a near infrared excitation Raman probe (Kaiser Optical Systems, Inc.). Spectra peak heights and peak areas were processed using in-house MATLAB® scripts. Expression of chondrogenic, angiogenic and osteogenic gene transcripts and osteogenic connective tissue progenitor cells (CTP-O) within the injured/healing muscle/soft tissue immediately surrounding the distal portion of the residual limb was determined by RT-PCR and osteogenic colony-forming cell assays (Colonyze™ image analysis software) under normoxic culture conditions (21% O_2), respectively.

Methods

a. Radiographic Micro-CT Analysis: Rats were anesthetized with isoflurane (2-4%) and imaged at POD-84 using a SkyScan 1176 in vivo high-resolution micro-CT (Bruker-MicroCT, Kontich, Belgium) with the following settings: 89-kV polychromatic x-ray beam, current of 256 µA, and an exposure time of 81 msec for each of

180 rotational steps. Three investigators (JGS, GJP and ATQ) independently reviewed the micro-CT images (170–200 flattened longitudinal micro-CT slices/rat) on a CT-Analyser (Bruker-MicroCT) and calculated the volume of ectopic bone formation using selected regions of interest on every fifth slice encompassing ectopic bone. The selected slices were used to generate a three-dimensional volume of interest, which was analyzed for the total volume of bone within the selected area.

b. Assay of osteoblastic connective tissue progenitor cells (CTP-O): The number of osteoblastic connective tissue progenitors in each sample was assayed using an established colony-forming assay. At various time points post injury, muscle-derived cells were isolated from muscle tissue immediately surrounding the amputation site. Tissue samples were cleaned from connective tissue, weighed, washed in PBS, minced into small pieces to create a fine slurry and then enzymatically dissociated with 300 U/ml of collagenase type II (Worthington, Lakewood, NJ) for 2 h at 37ºC. After incubation the enzyme was inactivated by adding 10% FBS. Next, the cell suspension was rigorously triturated (10-15x using a 5 ml pipette) to breakup large tissue fragments and release cells from intact fibers, and then washed to remove cell debris. Cells were resuspended in osteogenic medium consisting of alpha-minimum essential medium Eagle (α-MEM) with 10% fetal bovine serum, 100 U/mL penicillin, 100µg/mL streptomycin, 10^{-8} M dexamethasone, and 50 µg/mL ascorbate. Cell suspensions were serially filtered through 100µm and 70µm nylon filters then counted using a cellometer (Nexcelom Biosciences, St. Lawrence, MA). Cells were plated at a density of 250-4,000 cells/chamber (4.2 cm^2; Labtek chamber slides) CO_2 with medium changes on days 1, 3 and 5. Cells were cultured under standard conditions (37°C, 20% O_2, 5% CO_2, 95% humidity). Day 6 cultures were fixed with 1:1 acetone:methanol for 10 min and stained for nuclei (4,6-diamidino-2-phenylindole [DAPI]) and alkaline phosphatase (AP) as a marker for the preosteoblastic activity. Chambers were scanned and analyzed using Colonyze™ software, identifying colonies containing eight or more cells in a cluster. CTP-O prevalence (pCTP-0) was defined as the number of CTP-Os per 10^6 cells plated. Total CTP concentration was defined as the number of CTP-Os per gram of muscle tissue.

c. RNA isolation and gene expression: At indicated time points, skeletal muscle tissue collected from the extremity wound, specifically surrounding the amputation site (not set against the bone), and the corresponding distal quadriceps muscle of the contralateral limb were harvested and stored in RNALater (Ambion Inc, Austin, TX, USA) at 4ºC. Skeletal muscle samples obtained from age-matched naïve uninjured rats (n=4) served as control tissue. Total RNA was isolated and purified muscle cell lysates using RNeasy columns and DNase-I kits (Qiagen, Valencia, CA, USA) according to the manufacturer's protocols. RNA was stored at –80°C in nuclease-free water (Bio-Rad, Hercules, CA, USA). Total RNA was quantified spectroscopically by using NanoDrop 1000 (ThermoFisher Scientific, Waltham, MA) and RNA integrity/quality was assessed by microcapillary electrophoresis using an Agilent 2100 Bioanalyzer (Agilent Technologies, Santa Clara, CA). Reverse transcriptase polymerase chain reaction (RT-PCR) was used to convert 1 µg of RNA to cDNA. mRNA transcripts for 83 key genes involved in early chondrogenic, osteogenic and angiogenic signaling pathways (see Supplementary Table 1 for the complete list of genes and their function) were examined by real-time PCR using a custom low density microarray (Bio-Rad Laboratories, Hercules, CA) [16]. Relative gene transcript expression was calculated using the 2-ΔΔCt method and normalized and compared to the gene expression levels of non-injured rat muscle tissue. Gene transcripts values that were significantly deferentially expressed between treatment groups are reported.

d. Serum protein expression: At indicated time points, serum inflammatory mediators were measured using Luminex (Luminex Corporation, Austin, TX) multianalyte profiling technology (Bio-Plex ProTM rat cytokine assay kit; Bio-Rad Laboratories, Hercules, CA) according to the manufacturer's instructions. The concentrations of 9 serum inflammatory markers including: interleukin (IL)-1β, IL-6, IL-10, IL-12p70, IL-17, macrophage inflammatory protein (MIP)-1α, RANTES (regulated on activation, normal T cell expressed and secreted), tumor necrosis factor (TNF)-α, and monocyte chemoattractant protein (MCP)-1 were measured. The concentrations of all the analytes in the quality control reagents were found to be within the expected range. Results were extrapolated from each standard curve for each analyte.

e. Raman spectroscopy: At each time point, rats were euthanized and the intact soft tissue at the distal portion of the residual limb was examined via Raman Spectroscopy using a Kaiser Rxn1 PhAT probe 830 nm system (Kaiser Optical Systems, Inc., Ann Arbor, MI, USA) and 6 mm diameter excitation spot size. Dark subtracted and intensity-corrected spectra were each acquired using 5 second acquisitions and 15 accumulations under the cosmic ray removal function. Two repeat spectra were collected per animal in the same location. Reference spectra were acquired of harvested rat adipose tissue and naïve rat muscle and cortical bone. All processing of Raman data was performed in MATLAB® using custom-built scripts. Spectra were averaged per animal and smoothed using a seventh-order polynomial Savitzky-Golay filter, truncated to 600-1750 cm^{-1}, baseline subtracted using a fifth-order polynomial fitting routine, and normalized to the methyl/methylene scissoring band at 1445 cm^{-1}. Contribution of adipose tissue was removed from each spectrum using spectral subtraction of rat adipose reference signal. The contribution of mineralized tissue, particularly that of the underlying femur, was removed using spectral subtraction of rat cortical bone reference signal. Resulting spectra were analyzed for molecular markers of alterations in tissue composition characteristic of abnormal tissue pathology

f. Histology: For histological examination, cohorts of rats at the specified time points were euthanized (Fatal Plus 50 mg/kg IP; Patterson Veterinary, Devens, MA) and disarticulation of the hip was performed to collect the residual limb, which was washed with saline thoroughly then fixed in 10% neutral buffered formalin and subsequently decalcified in 5% formic acid. After complete decalcification, tissues were embedded in paraffin wax, cut into serial 5µm thick longitudinal sections using a microtome and mounted onto glass slides for histology. Sections were stained using hematoxylin-eosin (H&E) and Masson's trichrome using standard methods (Histoserv, Inc., Germantown, MD).

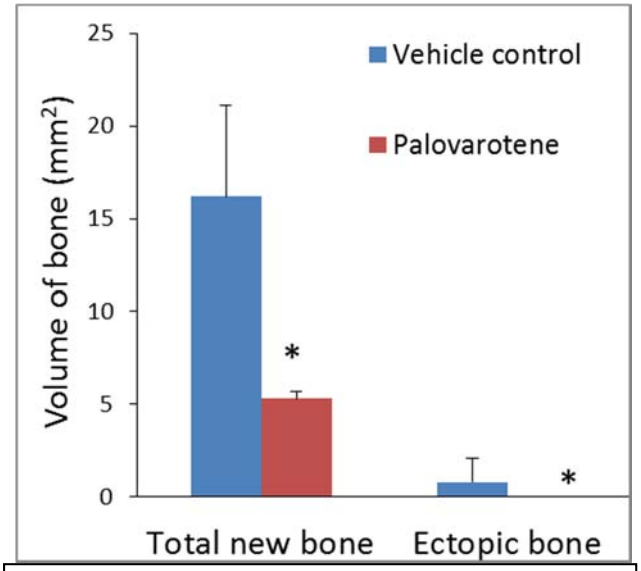

Figure 16. Palovarotene treatment inhibits heterotopic ossification. Analysis and quantification of total new bone and soft tissue ectopic bone volume using the flattened µ-CT images at 84 days after blast, extremity injury, and amputation (*= p <0.05 using the Welch's

g. Immunostaining analysis: Immunohistochemical analysis was performed on paraffin sections for Sox-9, PDGFr, UCP-1, substance-P, Tie-1, and osterix (Histoserve). Sections were de-waxed, rehydrated and retrieved using a Citrate pH 6.0 solution (40 min at 98°C). Endogenous peroxidase activity was quenched with a Methanol/H_2O_2 1.5% solution (20 min at room temperature (RT)). Primary rabbit anti-rats antibodies (Abcam, Cambridge, MA) were incubated overnight at RT in a humid chamber and processed with a non-biotin peroxidase-amplified system (Novolink, Novocastra Lab) according to the manufacturer's instructions. The immunological reaction (chromogen visualization) was visualized with 3-30 diaminobezidine tetrahydrochloride (DAB)/H_2O_2 solution. Sections were counterstained with haematoxylin, dehydrated and mounted in VectaMount (Vector Laboratories, Burlingame, CA).

Results

Early Delivery of Palovarotene Reduces Ectopic Bone Formation .

Palovarotene treatment significantly suppressed total new bone (16.2 ± 4.9 mm^3 to 5.3 ± 1.3 mm^3, p= 0.02; 67% mitigation) and ectopic bone (0.6 ± 0.4 mm^3 to 100% inhibition; p= 0.04) formation (Figure 16.).

Early Palovarotene Treatment Suppresses Osteoblastic Connective Tissue Progenitor Cell prevalence in injured/healing muscle tissue following trauma-induced extremity injury. Lower prevalence of osteogenic CTPs was measured in muscle tissue collected from Palovarotene-treated rats as compared to vehicle-treated rats (Figure 17.).

- Muscle-derived nucleated cells were isolated from the residual injured limbs of rats at various time points following blast-related polytraumatic injury and MRSA inoculation using our established blast-related HO model.
- Rats received daily via oral gavage (100 µl total volume) a single dose of either vehicle control (5% DMSO in corn oil) or Palovarotene (1.0 mg/kg).
- The rats were euthanized at 1, 3, 7, 10, 14 and 21 days post injury and the muscle derived progenitor cells were cultured for 7 days at 21% oxygen tensions and under culture conditions promoting the osteogenic differentiation of connective tissue progenitor cells (CTPs).
- The number of CTP colonies per 1 x 10^6 viable cell plated was determined ("prevalence')

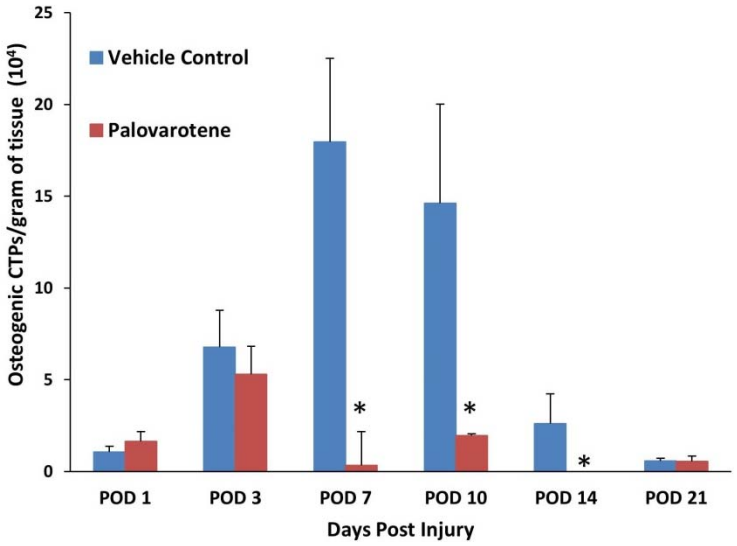

Figure 17. Palovarotene treatment significantly suppresses osteoblastic progenitor cell activity at the site of injury (*= p <0.05 using the Welch's two Sample t-test).

- In general there seems to be a trend towards a lower prevalence of osteoblastic CTPs in the injured soft tissue of rats treated with RAR- γ agonist in comparison to rats treated with vehicle control.
- Moreover, the absolute number of CTP-O/gram of tissue was significantly decreased in Palovarotene-treated rats POD-7 (p =0.01) and POD-10 (p =0.049) (Figure 17.).

C. Effects of Palovarotene Treatment on CTP-O Progenitor Cell Mobility and Proliferation. Colony density describes cell mobility.

Highly dense colonies show cells which have not traveled far from the original progenitor, and have formed a tight group. Less dense colonies show cells with high mobility. In both POD 7 and POD 10, where we found significant differences between the control and treatment groups, the control group showed higher cell density than the treatment. There is no noticeable trend in either the control or treatment groups in colony density over the course of the study. This figure describes the comparison of the median colony area (mm2) between Vehicle Control/ Corn oil+DMSO and the Palovarotene/RARgamma agonist treatment in of mouse muscle progenitor cell progeny. Results indicated that in POD 3, there is a significant difference (*= p <0.05 using the Welch's two Sample t-test) between the control and treatment. (Figure 18).

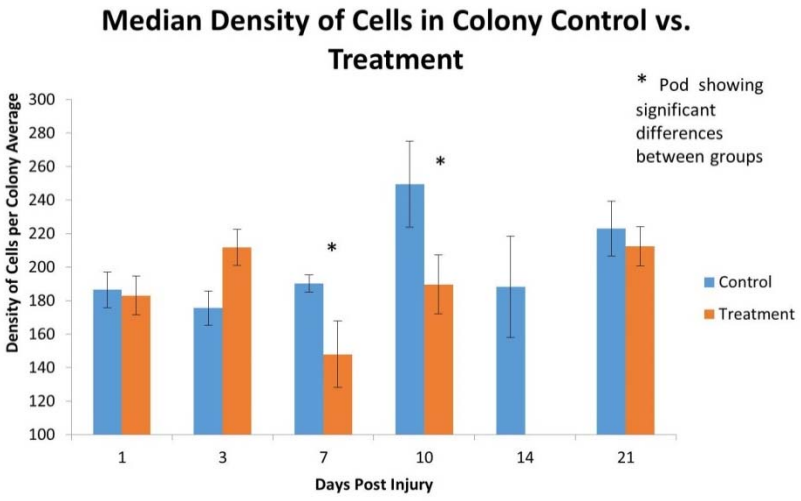

Figure 18.. Palovarotene treatment significantly suppresses osteoblastic progenitor cell mobility of cells isolated from muscle tissue at the site of extremity injury. There was a significant difference in cell density both POD 7 and POD 10 colonies (*= p <0.05 using the Welch's two Sample t-test).

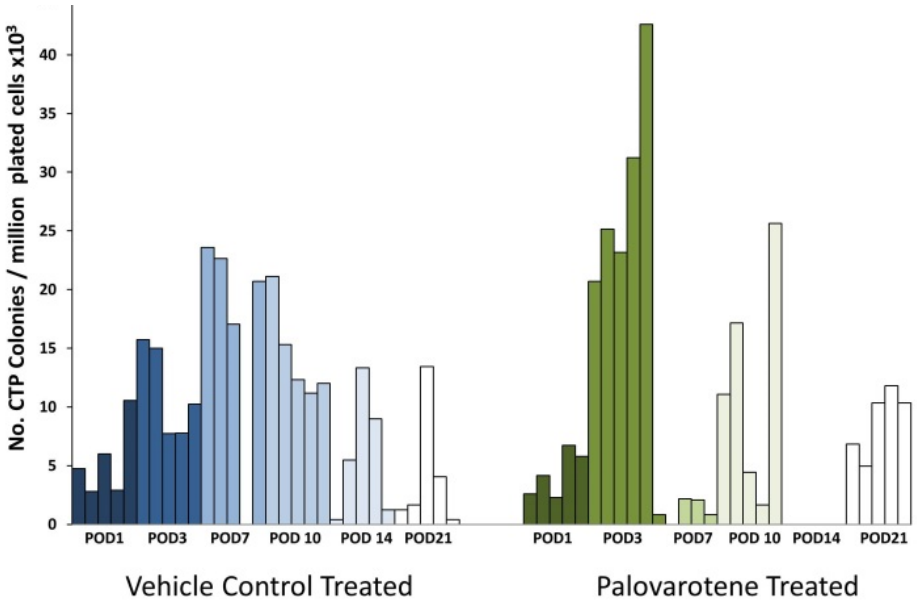

Figure 19. Palovarotene treatment decreases the prevalence of osteoblastic progenitor cell activity at the site of injury. Prevalence of CTP per 10^6 plated cells for all 60 rats (30 vehicle control and 30 Palovarotene treated rats in normoxic (20-21%) O_2 tension.

Colony size is a representation of both a cells doubling speed and their mobility (Figure 19.). The data seems to indicate that in the control, colony size peaks at day 3 before decreasing at later time points, showing similar size to the treatment. It's possible that the treatment limited this in the initial days post injury but that overtime, its effect was diminished.

Evidence of early osteogenesis in osteoblastic progenitor cells is measured by robust alkaline phosphatase (ALP) expression, as it inevitably leads to mineralization. ALP is among the first functional genes expressed in the process of calcification. We recorded the area of ALP staining within a colony over the total cell area within that colony (Figure 20). We found no significant differences.

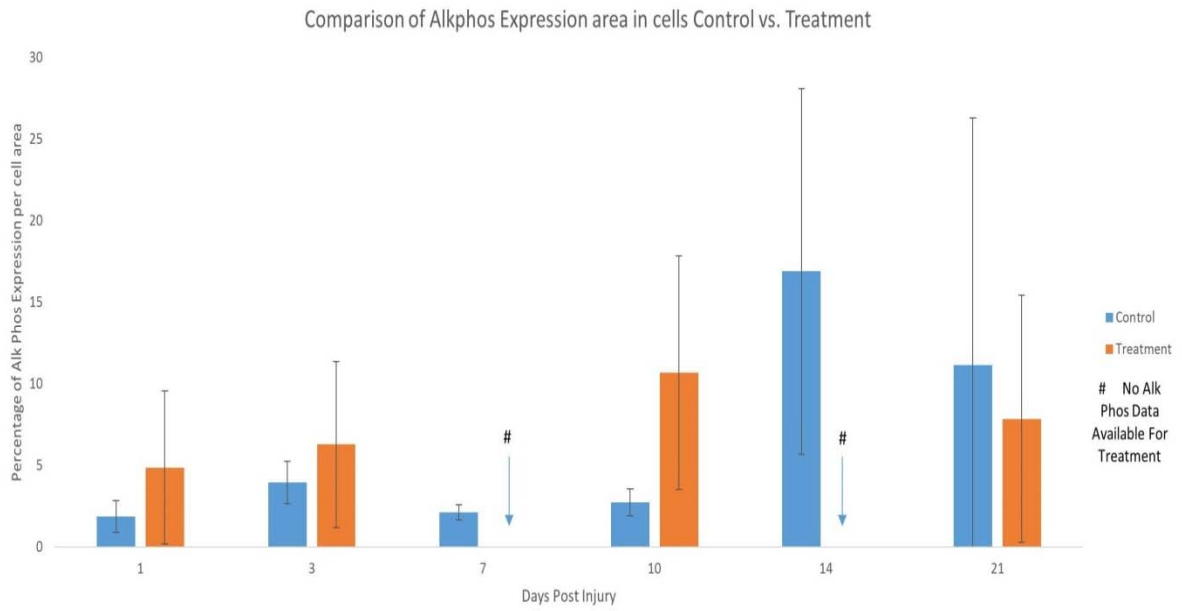

Figure 20. Palovarotene treatment had no significant effect on early mineralization potential of culturable tissue derived connective tissue progenitor cells.

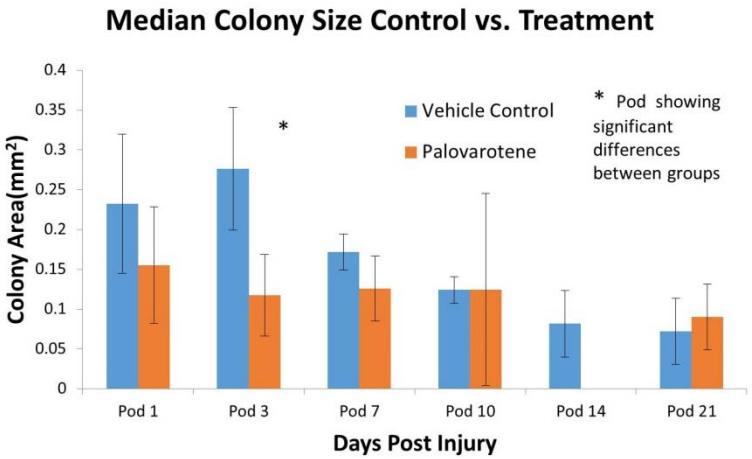

Figure 21. Palovarotene treatment significantly suppresses osteoblastic progenitor proliferation of cells isolated from muscle tissue at the site of extremity injury. The data indicated a significant difference in the median number of colony cells at POD 7 (*= $p < 0.05$ using the Welch's two Sample t-test).

The number of cells within a single osteoblastic cell colony is a parameter measuring cell doubling exclusively (Figure 21.). The data indicates that proliferative capacity of cultured osteoblastic cells was reduced with Palovarotene treatment for the initial days post treatment when compared to the muscle-derived osteoblastic progenitor cells cultured from vehicle control-treated injured rats. Subsequent time points showed a similar number of cells. The control group showed a gradual decrease in colony size over time. Colony size show limited change in the treatment, Figure 22.

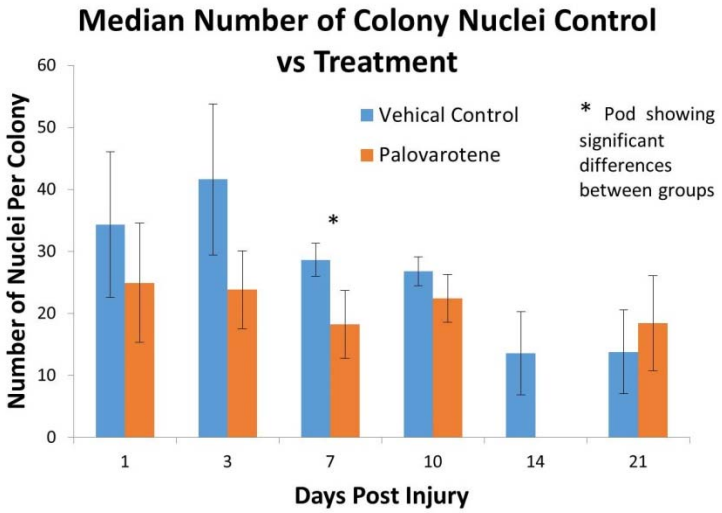

Figure 22. This figure describes the comparison of the median colony area (mm^2) between Vehicle Control/ Corn oil+DMSO and the Palovarotene/RARgamma agonist treatment in of mouse muscle progenitor cell progeny. Results indicated that in POD 3, there is a significant difference (*= $p < 0.05$ using the Welch's two Sample t-test) between the control and treatment.

Early Palovarotene Treatment has a Global Suppressive Effect on Trauma-induced Systemic Inflammation and Key Osteogenic, Chondrogenic and Angiogenic Pathway Genes that Regulate Endochondral Bone Development. Consistent with the cellular observations noted above, Palovarotene treatment resulted in significantly reduced serum levels (IL-1α, IL-1β, IL-6, IL-10, IL-18, TNF-α, VEGF, G-CSF, GM-CSF; $p<0.05$) at POD-10 in comparison to vehicle control-treated rats. Palovarotene treatment, also, significantly suppressed the expression of several trauma-induced osteoblast specific genes (alkaline phosphatase, *ALPL*; p=0.02 at POD-1 and POD-7, bone morphogenic protein 2, *BMP2;* p=0.0001 at POD-3, bone morphogenic protein 4, *BMP4;* p=0.005 at POD-1, osteopontin, *OPN*; p=0.02 at POD-1 and p=0.04 on POD-7, Smad Ubiquitination Regulatory Factor 1; *SMURF1*; p=0.03 at POD-3 and Smad ubiquitination regulatory factor 2; *SMURF2;* p=0.03 at POD-1), chondrogenic specific genes (cartilage oligomeric matrix protein; *COMP*; p=0.001 at POD-1) and angiogenic specific genes (vascular endothelial growth factor-A; *VEGF-A*; p=0.01 at POD-1 and p=0.02 at POD-3, vascular permeability factor receptor 1; (*FLT1*; p=0.01 at POD-1, vascular permeability factor receptor 2; *KDR*; p=0.04 at POD-3, endoglin; *ENG*; p=0.002 at POD-1) and hypoxic inducing factor 1-α; *HIF-1α*; p=0.002 at POD-1). (Figure 23 and 24.)

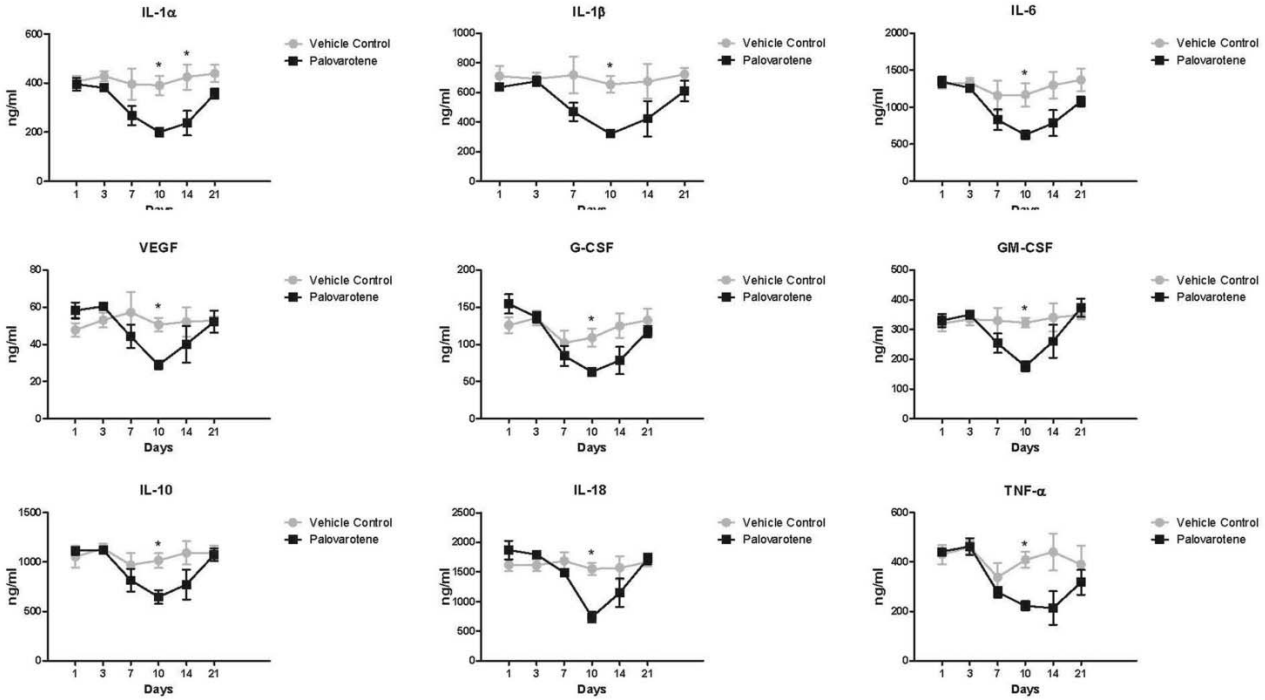

Figure 23. Palovarotene treatment attenuates blast-related extremity trauma induced systemic inflammation. At various time points post injury, serum levels of proinflammatory cytokine and chemokines were assayed by Luminex technology. Values are shown as mean ± SEM. * $p < 0.05$ using Student's *t*-test.

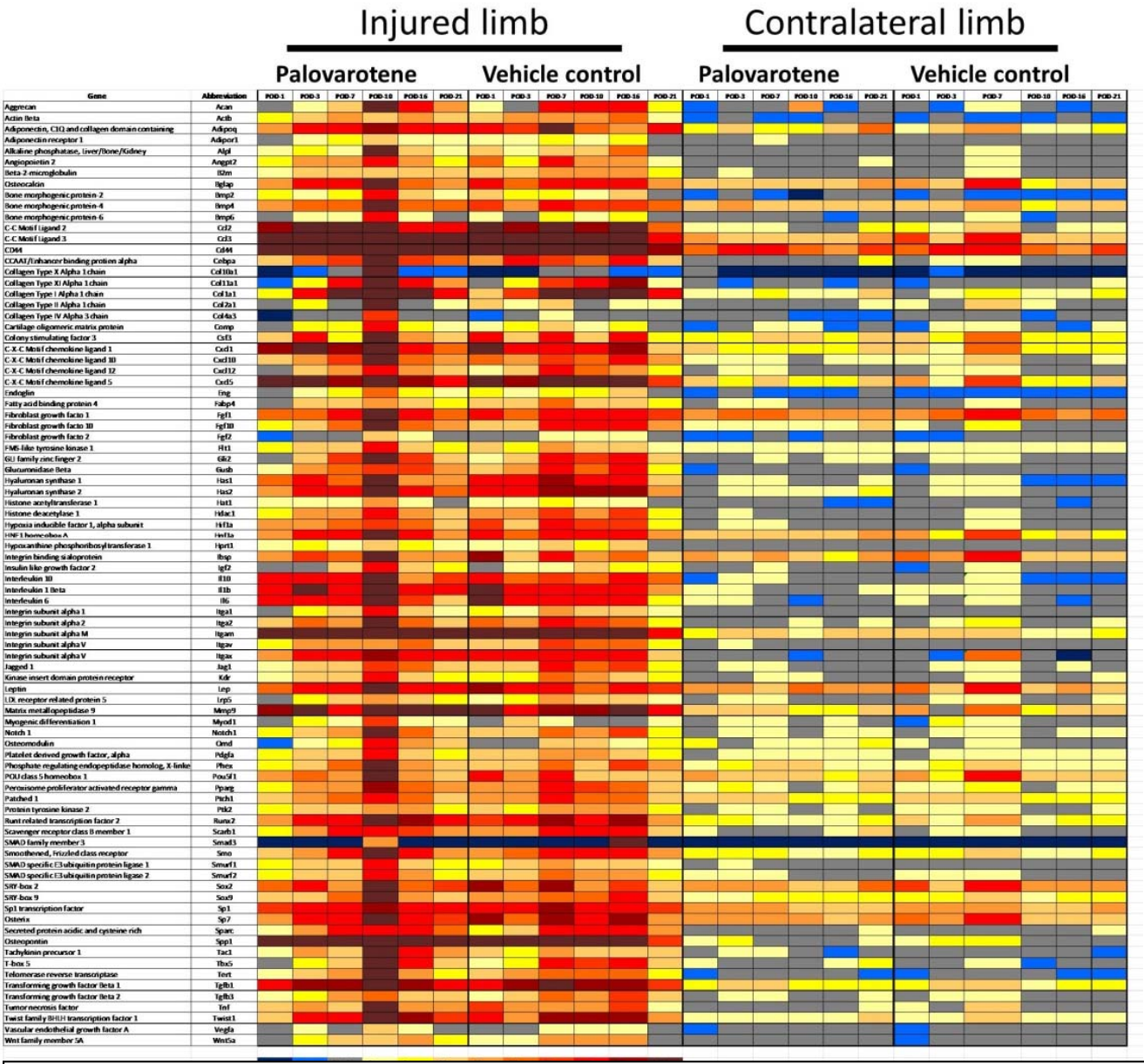

Figure 24.. Heat map depicting the relatedness of the chondrogenic, osteogenic and angiogenic gene expression profiles of injured muscle tissue from rats treated with Palovarotene-treated versus vehicle control .

Raman Spectroscopy Molecular Fingerprinting is a Sensitive Diagnostic Screening Tool for Detecting Chemical Changes in the Early Developmental Stages Associated with Trauma-induced Ectopic Bone Formation. Adipose subtracted Raman spectra at the site of amputation in a combat-trauma induced rat model of HO demonstrate tissue changes as early as POD 1 for both treated and untreated rats when compared to naïve muscle. For vehicle control animals, the Amide III band at 1240 cm^{-1} is increased and broadened and Amide III band 1270 cm^{-1} band decreased indicative of marked protein disorder and digestion following muscle trauma (Figure 25, left, grey arrow). For Palovarotene treated animals, changes to 1240 and 1270 cm^{-1} Amide III bands are minor and the appearance of a third band centered around 1285 cm^{-1} may represent a chemical marker of deviation in pathology (Figure 25, right, grey arrow). Raman intensity indicative of hydroxyapatite bone mineral 958 cm^{-1} within these experiments is attributable to both HO mineral and the signaling from the underlying femur due to the rather thin soft tissue coverage at the site of amputation and the sampling depth capability of our Raman probe. Bone mineral signal is greatly reduced in Palovarotene treated rats at POD 21 due to both reduced HO formation and reduced tissue necrosis of the soft tissue overlying the femur compared to vehicle control animals.

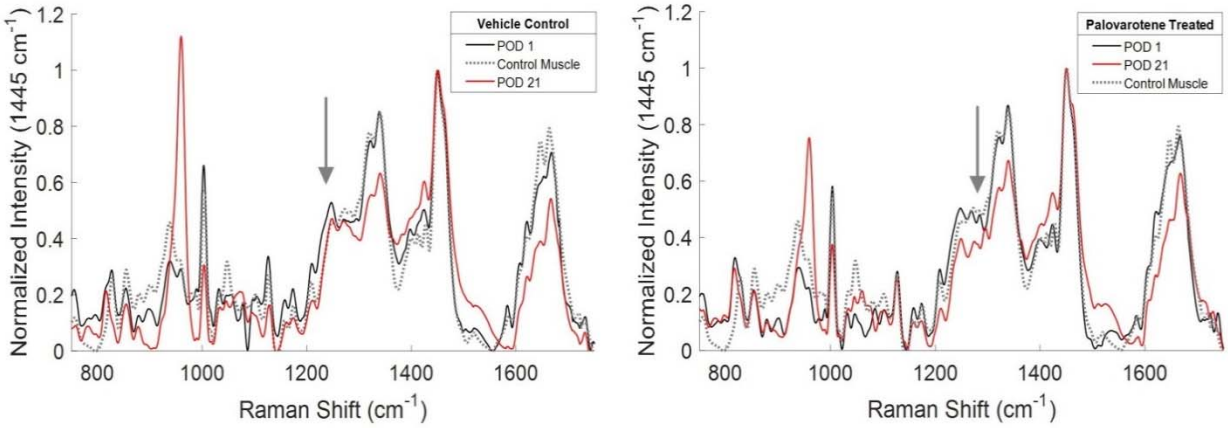

Figure 25. Mean adipose subtracted Raman spectra of vehicle control (left) and Palovarotene treated rats (right) at PODs 1 (black) and 21 days (red), and naïve muscle (grey dash).

Adipose and bone subtracted Raman spectra at the site of amputation in a combat-trauma induced rat model of HO demonstrate the composition of non-mineralized, damaged soft tissue in the days following injury. Spectroscopically determined changes in collagen content of the remaining soft tissue, an increase in spectral intensity and area in the Amide III bands (1240 and 1270 cm^{-1}), suggest early bone formation and chondrogenesis beginning between POD 3-7 in vehicle control rats when compared to naïve animals (Figure 26). This effect is suppressed in Palovarotene treated animals. Vehicle control animals exhibit decreased muscle content by POD 10 as evidenced by a reduction in CH_2CH_2 wag bands at 1340 and 1370 cm^{-1} signaling a transition from the strongly helical protein secondary structure of actin containing muscle tissue to increased β–sheet/disorder protein structure of collagen. In fact, the replacement of muscle with collagen can be interpreted as an early sign of tissue endochondral ossification. Histologically, for untreated rats, at day 7 post injury thick fibrosis, hemorrhage, marked necrosis, and the presence of proliferative and hypertrophic chondrocytes are observed, and the formation of vascularized hyaline cartilage is observed around POD 7-10. Spectroscopic data suggests early collagen formation and early muscle necrosis is reduced in Palovarotene treated animals within ten days post injury. This is confirmed by macroscopic thinning of muscle tissue coverage at the amputation site by POD 10 in untreated animals and results presented in Figure 26. Histologically, for untreated rats hyaline cartilage begins to be replaced with osteoid by POD 14, and signs of immature woven bone are present. The transition to mineralization is not evident in Raman spectra in Figure 3 as spectral subtraction of cortical bone removes spectral signatures of both mature bone related mineral and matrix proteins. Palovarotene treated animal tissue histology indicates increased

muscle fibrosis by POD 14. Therefore, remaining soft tissue at the site of amputation exhibits only minor spectral differences in treated and untreated animals in adipose and bone mineral subtracted spectra. At POD 21, Amide III bands are increased for untreated rats compared to treated and may indicate further collagen production in the remaining soft tissue as HO development spreads.

Spectroscopic markers of altered collagen production were observed at within one week from injury in both human and a blast combat trauma model of HO. Spectral signatures of collagen and HO formation were reduced in Palovarotene rats. As collagen deposition is associated with normal re-epithelialization of the wound bed, Raman spectroscopy of early HO emphasizes the need to explore the relationship of altered collagen production in response to trauma and its role in HO development. Raman spectroscopy may serve as an important tool in monitoring HO development in both future animal and human work and serve as a non-invasive tool to aid in the surgical excision at HO tissue margins.

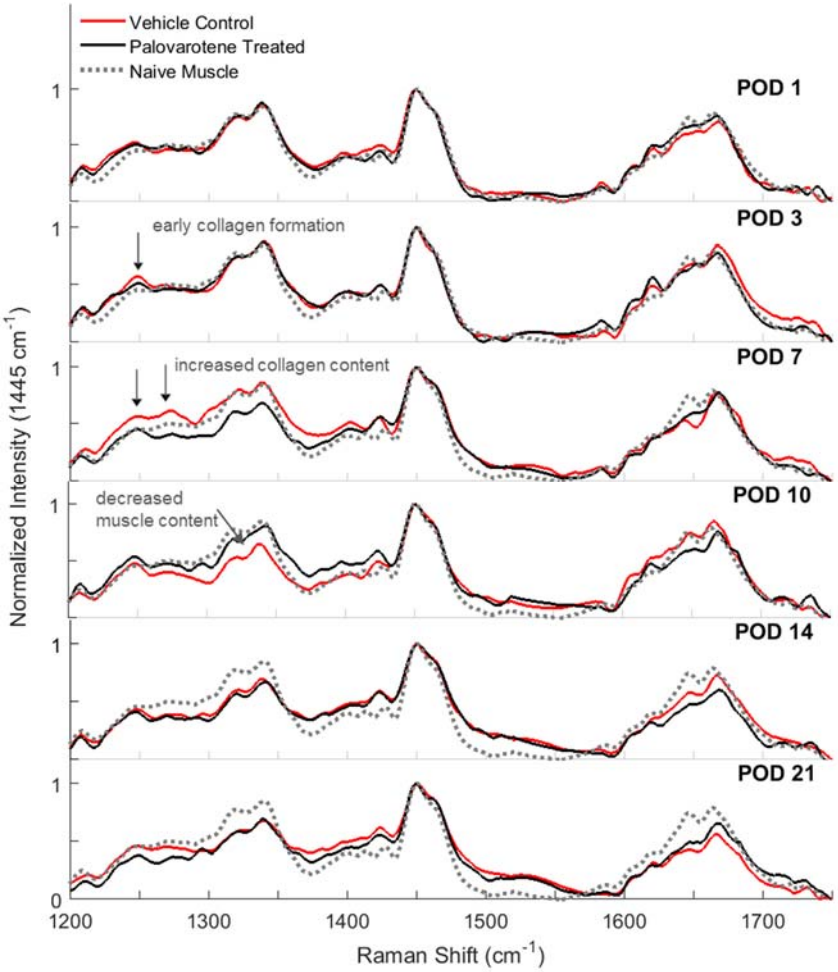

Figure 26. Mean adipose and cortical bone subtracted Raman spectra of untreated and Palovarotene treated rats at time points 1, 3, 7, 10, 14, and 21 days post injury

Palovarotene Suppresses Early Chondrogenic and Osteogenic Differentiation

In this set of studies we investigated how Palovarotene treatment alters the tissue environment and influences the osteogenic potential of muscle connective tissue progenitors (CTP-O) resulting in attenuated heterotopic ossification (HO). We performed Masson's trichrome staining and immunohistochemistry on lesional tissue from injured residual limbs using antibodies specific for the Osterix (SP7), PDGFr, Sox-9, Tie-1 and substance-P (SP) to detect osteoblastic, chondrogenic and vascular endothelial progenitors.

We collected affected tissues around the amputated area of the limbs at day 14 from the initial blast injury and

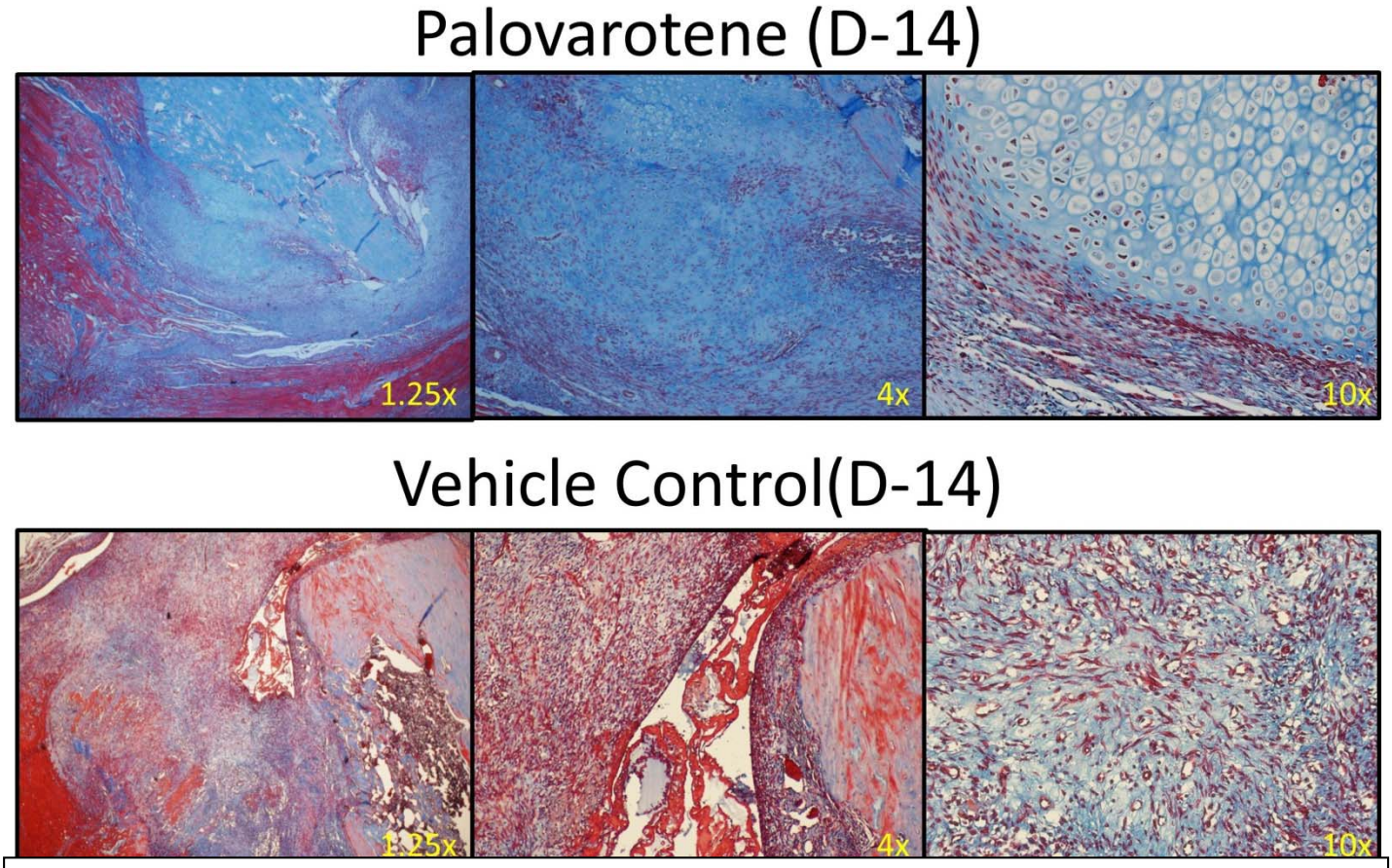

Figure 27: Representative sections of the limb amputation site at POD-14 from Palovarotne-treated and vehicle control treated injured rats stained with Masson's trichrome, where blue staining indicates sites of active chondrogenesis and/or fibrosis.

processed them for histochemical analyses. In vehicle control samples, the amputated area at days 14 displayed obvious signs of an ongoing and active endochondral ossification process, with foci of immature and hypertrophying cartilage, numerous surrounding cells exhibiting progenitor characteristics, acidophilic osteoid matrix and early evidence of immature woven bone (Figure 27). In comparison, specimens obtained from Palovarotene-treated rats showed clear decrease in the amount of detectable immature cartilage and vascularized hypertrophying cartilage.. In place of these skeletogenic tissues, we invariably observed the presence of extensive areas of fibrous connective tissues that were particularly obvious at day 14 post injury. Histological investigation showed that the medullary cavity was largely capped/filled with similar fibrous connective tissue rather than new bone.

The decreased expression of Osterix, PDGFr, Sox-9, and Tie-1 positive cells in Palovaroten-treated rats suggests an overall suppressed response to osteoblast, chondrogenic and angiogenic differentiation. Osterix, PDGFr, Sox-9, and Tie-1 cells expression were confined to areas where early pre-osseous lesions were chondrocyte to osteoblast transition was evident. Of importance immature fibroblasts within the injured/healing tissue were typically positive for PDGFr. Osterix, PDGFr, Sox-9, and Tie-1 positive cells were never observed in healthy muscle tissue. These results are consistent with the CTP-O progenitor, gene expression and raman spectral imaging findings described above. (Figure 28).

Substance P is a neuropeptide mediating response to pain and produced by neurons, osteoblasts and macrophages in injured and has been identified in active areas of bone regeneration following fracture and in early ectopic bone development. SP has a proinflammatory effect and has been shown to promote the extravasation, migration, and accumulation of inflammatory leukocytes and regenerative tissue progenitor cells at sites of tissue injury. We found that appreciable SP expression was only detectable in injured muscle tissue from vehicle control treated rats.

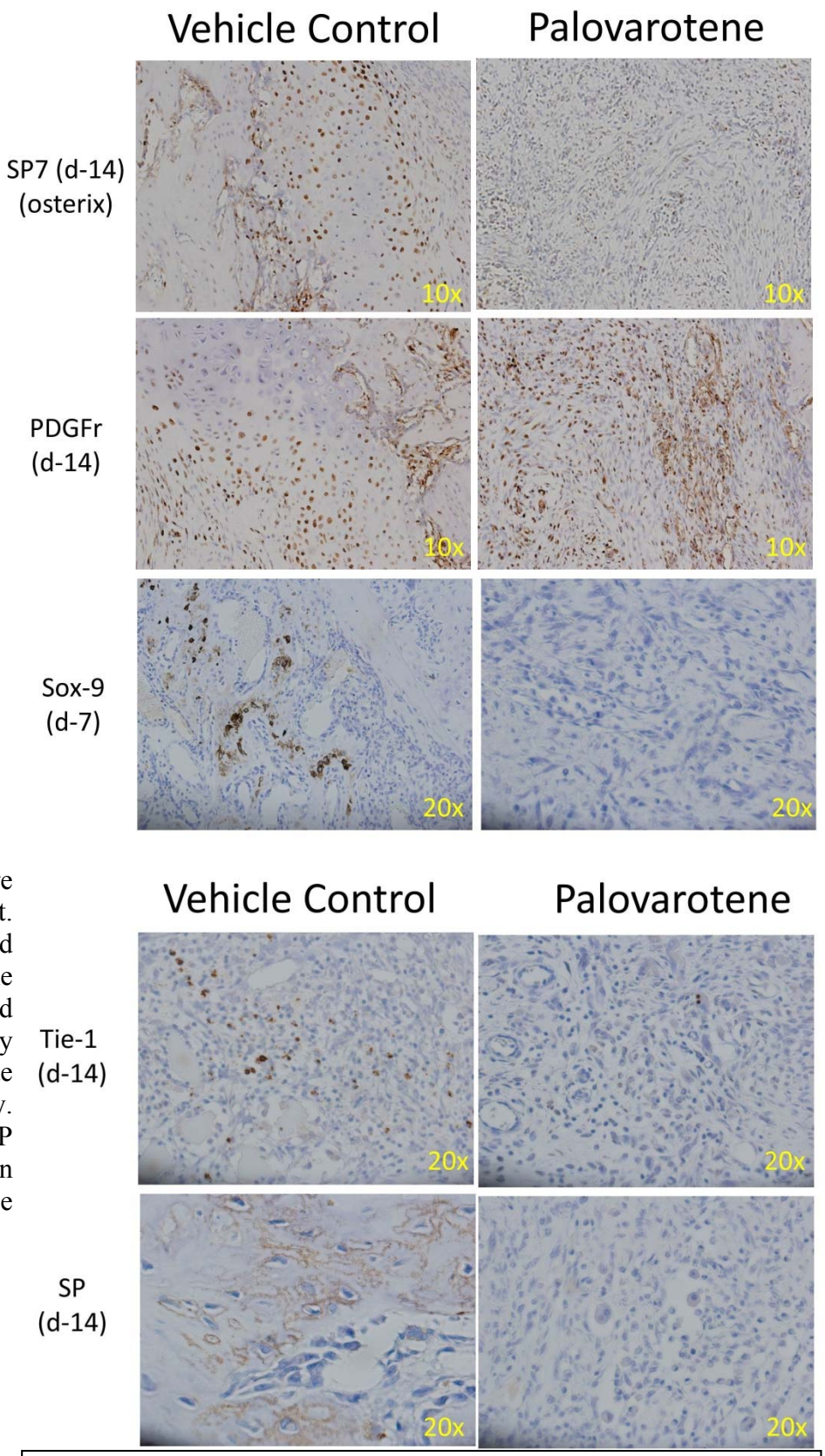

Figure 28: Representative sections of the limb amputation site at POD-3 or POD-14 from Palovarotne-treated and vehicle control treated injured rats stained for osterix (SP7), PDGFr, Sox-9, Tie-1 and substance P (SP).

HA expression in cultured cells from injured rats and their response to treatment with Palovarotene

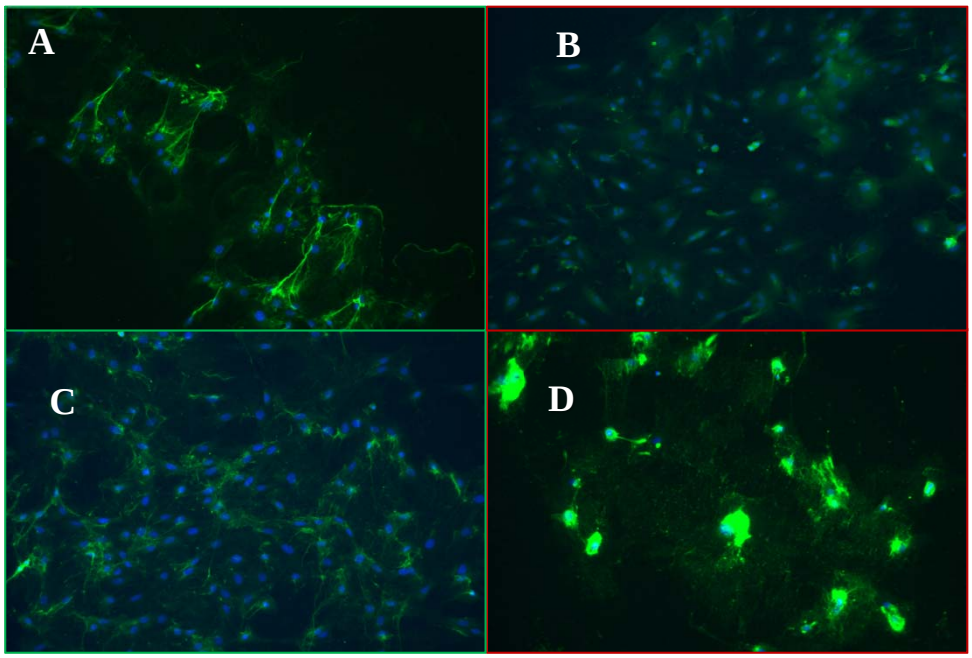

Figure 29 (A-D): Vehicle control rat culture stained with HABP Non-Permeabilized cells (A) show extracellular HA (green) with cables connecting to nuclei (blue) and Permeabilized cells show no clear internal localization (C). Palovarotene treated rat culture stained with HABP Non-Permeabilized cells (B) show no significant extracellular HA while permeabilized cultures (D) show perinuclear intracellular HA.
The rats were subjected to a blast overpressure (BOP) model designed to induce Heterotopic Ossification. Rats were then force fed with either a vehicle control corn oil + DMSO supplement or Palovarotene. Muscle tissue at the distal portion of the amputation site was collected and processed for cell culture. Cells were grown in culture for 6 days and fixed with formalin + 0.05% CPC.

Primary rat muscle cell cultures were stained with Hyaluronan Binding protein (HABP) coupled with Streptavidin Alexa Fluor 488 conjugate (green), and DAPI (blue). HABP is a large protein that selectively binds to HA but cannot enter the cell due to its size. Therefore only extracellular HA is labeled unless the cells are permeabilized with Triton x100.

Cells from injured rats treated with Control (A and C): These images show that HA is secreted into the extracellular matrix formed by cells from injured rats when cells are exposed to only control vehicle. (Figure A). HA cables are seen running between nuclei, consistent with the HA synthesis that has been associated with an inflammatory response. In contrast, cultures from non injured control rats showed no extracellular HA (data not shown), and when permeabilized, the cells do not reveal significant intracellular HA and HA cables are less defined.

Cells from Injured rats treated with Palovarotene (B and D): Palovarotene treated cells show little to no extracellular accumulation of HA, and no obvious cable formation (Figure B). After permeabilization, intracellular perinuclear localization of HA can be seen (Figure D).
The difference in HA response after treatment with Palovarotene may be biologically important. Further work will be required to define the mechanism behind this finding and its potential clinical importance.

CONCLUSIONS - Aim 4

We demonstrate that retinoid-dependent and retinoic acid receptor (RAR)-mediated mechanisms play a key role in trauma-induced ectopic endochondral bone formation. Palovarotene mediated mitigation of trauma-induced ectopic bone formation is associated with significantly reduced inflammatory, chondrogenic, angiogenic and osteogenic mediator signaling. In addition, Palovarotene treatment, when given the day after injury, reduced the local increase in the number of colony founding CTP-Os at 3, 7 and 10 days. This suggests a possible direct effect in inhibiting proliferation CTP-O progenitors as a mechanism underlining the drug's anti chondro-angio-osteogenic properties.

Significance

By preventing the HO formation completely, we aim to change our current paradigm of HO management from one of delayed diagnosis and surgical extirpation to one of primary prevention. This treatment may benefit injured service members with delayed evacuation given the opportunity to deploy prophylaxis in forward units.

4. KEY RESEARCH ACCOMPLISHMENTS

- Specific Aims 1, 3 and 4 completed.
- ORS 2017 abstract accepted (see appendix)
- Papers summarizing work in Aim 1, 3 and 4 are in preparation
- Effective methods for using tissue histology, cytokine analysis, cell analysis, Raman spectroscopy and ultrasound may provide clinical tools for predicting if or where HO will occur.
- The limited number of patients available for inclusion in this assessment prevented definitive testing of these methods.
- Effective protocols for tissue sampling and analysis have been established.
- Glucose and Heparin have been identified as potentially clinically relevant as accessible modulators of bone formation in vitro.
- Palovarotene has been identified as a potentially clinically relevant and accessible modulator of bone formation in vivo, using the rat blast injury model developed at WRNMMC.

5. CONCLUSION

- **Effective methods and protocols for tissue sampling and analysis have been established.** The data generated in this study provides a valuable description of the characteristics of the data set that would be obtained in future studies that can extend this work, (see bulleted list below), including the range of values and confounding technical issues that need to be managed.

    - We could compare four patient biopsy sites which were negative to four that were positive, and identify genes that appeared to be differentially expressed (Table 2.). However, this hypothesis that relatively levels of gene expression could be used to predict HO formation could not be tested in this very limited sample size.
    - Colony forming efficiency (CFU) in the patient muscle-derived progenitor population of wound site biopsy samples increased when samples were cultured under 21% O_2 tension, although these data were not statistically significant.
    - We observed an increasing but non-significant trend for a higher colony forming efficiency prevalence in biopsy samples cultured at 21% O_2 tension, for wound tissue sample in sites that eventually become HO positive sites.

- Both glucose and heparin represent low toxicity agents that are worthy of further evaluation as tools for local suppression of CTP activation and proliferation and subsequent bone formation following blast injury
- Raman spectroscopy may serve as an important tool in monitoring HO development in both future animal and human work and serve as a non-invasive tool to aid in the surgical excision at HO tissue margins.

6. PUBLICATIONS, ABSTRACTS, AND PRESENTATIONS

a.

1 Lay Press: Nothing to Report
2 Peer-Reviewed Scientific Journals: Nothing to Report
3 Invited Articles: Nothing to Report
4 Abstracts: Ammar T Qureshi[1], Jonathan G Seavey[1,2], Katherine E Cilwa[1], Allison M Tomasino[1], Wesley Bova[3], Cynthia Boehm[3], Erin M Sanders[1], Devaveena Dey[1], Jonathan A Forsberg[1,2], George Muschler[3] and Thomas A Davis[1,2] [1]Regenerative Medicine Department, Naval Medical Research Center, Silver Spring, MD, [2] Department of Surgery, Uniformed Services University and the Walter Reed National Military Medical Center, Bethesda, MD, [3] Department of Biomedical Engineering, Cleveland Clinic, Cleveland, OH. **Palovarotene Treatment Suppresses Osteoprogenitor Cell Activity and Ectopic Bone Formation in a Trauma Induced Rodent Model of Heterotopic Ossification,** poster presentation at the Annual meeting of the Orthopaedic Research Society, San Diego, CA. March 19-22, 2017.

b. Nothing to Report

7. INVENTIONS,PATENTS,AND LICENSES

a. Nothing to report

8. REPORTABLE OUTCOMES

- Effective methods for using tissue histology, cytokine analysis, cell analysis, Raman spectroscopy and ultrasound may provide clinical tools for predicting if or where HO will occur.
- The limited number of patients available for inclusion in this assessment prevented definitive testing of these methods.
- Effective protocols for tissue sampling and analysis have been established. The data generated here provides a valuable description of the characteristics of the data set that would be obtained in future studies that extend this work, including the range of values and confounding technical issues that need to be managed.
- Glucose and Heparin provide possible therapeutic molecules for modulation of HO. We have demonstrated that in vitro exposure to elevated glucose concentration (25mM rather than 5 mM) and sodium Heparin have separate and potentially synergistic effects in decreasing colony forming efficiency (CFE) among human bone-derived osteogenic connective tissue progenitors (CTP-Os). These agents may also decrease proliferation among CTP progeny and may speed the onset of differentiation. In contrast, increases in osmolarity of 20 mM did not change CFE nor proliferation. If these findings are confirmed in ongoing assessment, and pre-clinical assessment of topical, regional or systemic modulation or glucose and heparin may be considered in the rat model reported here.

- Palovarotene treatment of rats resulted in a decrease in bone formation. Palovarotene was also associated with decrease in the prevalence of CTPs in local tissues 1-2 weeks after injury, and in a reduction in mean colony size (proliferation) among the progeny of colony founding CTPs. Moreover, muscle injury sites in Palovarotene treated animals demonstrated significantly reduced serum levels (IL-1α, IL-1β, IL-6, IL-10, IL-18, TNF-α, VEGF, G-CSF, GM-CSF; $p<0.05$) at POD-10. Palovarotene treatment, also, significantly suppressed the expression of several trauma-induced osteoblast specific genes (alkaline phosphatase, *ALPL*; p=0.02 at POD-1 and POD-7, bone morphogenic protein 2, *BMP2;* p=0.0001 at POD-3, bone morphogenic protein 4, *BMP4;* p=0.005 at POD-1, osteopontin, *OPN*; p=0.02 at POD-1 and p=0.04 on POD-7, Smad Ubiquitination Regulatory Factor 1; *SMURF1*; p=0.03 at POD-3 and Smad ubiquitination regulatory factor 2; *SMURF2;* p=0.03 at POD-1), chondrogenic specific genes (cartilage oligomeric matrix protein; *COMP*; p=0.001 at POD-1) and angiogenic specific genes (vascular endothelial growth factor-A; *VEGF-A*; p=0.01 at POD-1 and p=0.02 at POD-3, vascular permeability factor receptor 1; (*FLT1*; p=0.01 at POD-1, vascular permeability factor receptor 2; *KDR*; p=0.04 at POD-3, endoglin; *ENG*; p=0.002 at POD-1) and hypoxic inducing factor 1-α; *HIF-1α*; p=0.002 at POD-1). These findings support consideration of Palovarotene treatment in a clinical trial for prevention or mitigation of HO following major extremity trauma.

9. OTHER ACHIEVEMENTS

Nothing to Report

10. REFERENCES

Specific Aim 1, Section H

1.) Bastow,E.R, Byers,S.,Golub, S.B.,Clarkin, C.E., Pitsillides, A.A., Fosang, A.J., 2008, Hyaluronan synthesis and degradation in cartilage and bone. Cell. Mole. Life Sci 65(2008) 395-413.

2.) Midura, R.J., X. Su, Morcuende, J.A., Tammi, M., Tammi,R., Parathyroid Hormone rapidly stimulates hyaluronan synthesis by periosteal osteoblasts in the tibial diaphysis of the growing rat. J.Biol. Chem. 278, 51462-51468

3.) Boskey, A.L., and Dick, B.L. (1991), Hyaluronan interactions with hydroxyapatite no not alter in vitro hydroxyapatite crystal proliferation and growth. Matrix 11, 442-446.

4.) Aya, K.L., Stern, R., Hyaluronan in wound healing: rediscovering a major player, Wound Repair and Regeneration, vol. 22, :5, 579-593

5.) Dunphy, JE , Wound Healing, *Surg Clin North Am*1978; **58**: 907–916

6.) Dunphy JE, Udupa KN Chemical and histochemical sequences in the normal healing of wounds. *N Engl J Med*1955*;* **253***:* 847–851.

Specific Aim 3

1.) Villarruel SM, Boehm CA, Pennington M, et al. 2008. The effect of oxygen tension on the in vitro assay of human osteoblastic connective tissue progenitor cells.J. Orthop. Res. 26(10):1390–7.

2.) Heylman CM, Caralla TN, Boehm CA, et al. 2013. Slowing the Onset of Hypoxia Increases Colony Forming Efficiency of Connective Tissue Progenitor Cells In Vitro.J. Regen. Med. Tissue Eng. 2.

3.) Powell KA, Nakamoto C, Villarruel S, et al. 2007. Quantitative image analysis of connective tissue progenitors.Anal. Quant. Cytol. Histol. 29(2):112–21.

4.) Friedenstein AJ, Deriglasova UF, Kulagina NN, et al. 1974. Precursors for fibroblasts in different populations of hematopoietic cells as detected by the in vitro colony assay method.Exp. Hematol. 2(2):83–92.

5.) Muschler GF, Boehm C, Easley K. 1997. Aspiration to obtain osteoblast progenitor cells from human bone marrow: the influence of aspiration volume.J. Bone Joint Surg. Am. 79(11):1699–709.

6.) Muschler GF, Nitto H, Boehm CA, Easley KA. 2001. Age- and gender-related changes in the cellularity of human bone marrow and the prevalence of osteoblastic progenitors.J. Orthop. Res. 19(1):117–25.

7.) Majors AK, Boehm CA, Nitto H, et al. 1997. Characterization of human bone marrow stromal cells with respect to osteoblastic differentiation.J. Orthop. Res. 15(4):546–57.

11. APPENDICES

Appendix 1. Selected chondrogenic, angiogenic and osteogenic-related genes evaluated using PCR (RT- PCR) low-density microarray assays

Gene Symbol	Accession #	Official Full Name	Function of Encoded Protein
Acan	NM_022190	Aggrecan	Extracellular matrix proteoglycan; cleaved by ADAMTS1.
Adipoq	NM_144744	Adiponectin, C1Q and collagen domain containing	Hormone secreted by adipocytes; regulates fatty acid catabolism and glucose levels.
Adipor1	NM_207587	Adiponectin receptor 1	Activation stimulates AMP-activated kinase signaling pathway, affecting levels of fatty acid oxidation and insulin sensitivity.
Alpl	NM_013059	Alkaline phosphatase, liver/bone/kidney	Tissue non-specific alkaline phosphatase. Exact function unknown; proposed to play role in matrix mineralization.
Angpt2	NM_134454	Angiopoietin 2	Disrupts the vascular remodeling ability of angiopoietin1; may induce endothelial cell apoptosis.
Bmp2	NM_017178	Bone morphogenetic protein 2	Acts as a disulfide-linked homodimer and induces bone and cartilage formation.
Bmp4	NM_012827	Bone morphogenetic protein 4	Plays an important role in endochondral bone formation; a reduction in expression has been associated with bone diseases including Fibrodysplasia Ossificans Progressiva
Bmp6	NM_013107	Bone morphogenetic protein 6	Secreted signaling molecules that can induce ectopic bone growth; proposed role in early development.
Ibsp	NM_012587	Integrin-binding sialoprotein	Major structural protein of the bone matrix, constituting approximately 12% of the noncollagenous proteins in human bone.
Cd44	NM_012924	CD44 molecule	Cell-surface glycoprotein involved in cell-cell interactions, cell adhesion, and migration.
Cebpa	NM_012524	CCAAT/enhancer binding protein (C/EBP), alpha	Modulates the expression of genes involved in cell cycle regulation and body weight homeostasis; associated with acute myeloid leukemia.
Col10a1	XM_001053056	Collagen, type X, alpha 1	Short chain collagen expressed by hypertrophic chondrocytes during endochondral ossification.
Col11a1	NM_013117	Collagen, type XI, alpha 1	Encodes one of the two alpha chains of type XI collagen, a minor fibrillar collagen.
Col1a1	NM_053304	Collagen, type I, alpha 1	Encodes pro-alpha1 chains of type I collagen, found in most connective tissues and abundant in bone, cornea, dermis and tendon.
Col2a1	NM_012929	Collagen, type II, alpha 1	Encodes alpha-1 chain of type II collagen, a fibrillar collagen found in cartilage and the vitreous humor of the eye.
Col4a3	NM_001135759	Collagen, type IV, alpha 3	Encodes alpha-3 subunit of type IV collagen, the major structural component of basement membranes.
Comp	NM_012834	Cartilage oligomeric matrix protein	Noncollagenous extracellular matrix protein containing EGF-like and calcium-binding domains.
Csf3	NM_017104	Colony stimulating factor 3 (granulocyte)	Cytokine controlling the production, differentiation, and function of granulocytes.
Cxcl1	NM_030845	Chemokine (C-X-C motif) ligand 1 (melanoma growth stimulating activity, alpha)	Secreted growth factor that plays a role in inflammation and acts as a chemoattractant for neutrophils.
Cxcl10	NM_139089	Chemokine (C-X-C motif) ligand 10	Binds to CXCR3 resulting in pleiotropic effects, including stimulation of monocytes, natural killer and T-cell migration, and modulation of adhesion molecule expression.
Cxcl12	NM_022177	Chemokine (C-X-C motif) ligand 12 (stromal cell-derived factor 1)	Plays a role in embryogenesis, immune surveillance, inflammation response, tissue homeostasis, and tumor growth and metastasis.
Cxcl5	NM_022214	Chemokine (C-X-C motif) ligand 5	Recruits neutrophils, promotes angiogenesis and remodels connective tissues.
Eng	NM_001010968	Endoglin	Major glycoprotein of the vascular endothelium and a component of the transforming growth factor beta receptor complex.
Fabp4	NM_053365	Fatty acid binding protein 4, adipocyte	Binds long-chain fatty acids and other hydrophobic ligands; also thought to play a role in fatty acid uptake, transport, and metabolism.
Fgf1	NM_012846	Fibroblast growth factor 1	Modifies endothelial cell migration and proliferation; acts as a mitogen for a variety of mesoderm- and neuroectoderm-derived cells in vitro.

Fgf10	NM_012951	Fibroblast growth factor 10	Exhibits mitogenic activity for keratinizing epidermal cells; implicated to be a primary factor in wound healing.
Fgf2	NM_019305	Fibroblast growth factor 2	Thought to be involved in limb and nervous system development, wound healing, and tumor growth.
Flt1	NM_019306	Fms-related tyrosine kinase 1	Member of the vascular endothelial growth factor receptor (VEGFR) family; plays an important role in angiogenesis and vasculogenesis.
Gli2	NM_001107169	GLI family zinc finger 2	Transcription factor that binds DNA through zinc finger motifs; localizes to the cytoplasm and activates patched Drosophila homolog (PTCH) gene expression.
Has1	NM_172323	Hyaluronan synthase 1	Constituent of the extracellular matrix space; actively produced during wound healing and tissue repair to provide a framework for ingrowth of blood vessels and fibroblasts.
Has2	NM_013153	Hyaluronan synthase 2	Current understanding suggests similar function as HAS2
Hat1	NM_001009657	Histone acetyltransferase 1	Involved in the rapid acetylation of newly synthesized cytoplasmic histones.
Hdac1	NM_001025409	Histone deacetylase 1	Regulates eukaryotic gene expression through histone deacetylation; also involved in control of cell proliferation and differentiation.
Hif1a	NM_024359	Hypoxia-inducible factor 1, alpha subunit (basic helix-loop-helix transcription factor)	Activates transcription of many genes in response to hypoxia, including those involved in energy metabolism, angiogenesis, apoptosis.
Hnf1a	NM_012669	HNF1 homeobox A	Transcription factor required for the expression of several liver-specific genes.
Igf2	NM_031511	Insulin-like growth factor 2	A member of the insulin family of polypeptide growth factors, which are involved in development and growth.
Il10	NM_012854	Interleukin 10	A cytokine with pleiotropic effects on immunoregulation and inflammation, including down-regulation of Th1 cytokine expression and enhanced B cell activity.
Il1b	NM_031512	Interleukin 1 beta	An important mediator of the inflammatory response, including effects on cell proliferation, differentiation, and apoptosis.
Il6	NM_012589	Interleukin 6	Endogenous pyrogen and inflammatory mediator produced at sites of acute and chronic inflammation; also involved in B cell maturation.
Tac1	NM_012666	Tachykinin 1	Encodes substance P, neurokinin A, neuropeptide K, and neuropeptide gamma, hormones thought to function as neurotransmitters interacting with nerve receptors and smooth muscle cells.
Itga1	NM_030994	Integrin, alpha 1	Heterodimerizes with beta 1 subunit to form a cell-surface receptor; is involved in cell-cell adhesion and may play a role in inflammation and fibrosis.
Itga2	XM_345156	Integrin, alpha 2	Heterodimerizes with beta subunit and mediates the adhesion of platelets and other cell types to the extracellular matrix.
Itgam	NM_012711	Integrin, alpha M	Involved in adherence of neutrophils and monocytes to stimulated endothelium, as well as in the phagocytosis of complement coated particles.
Itgav	NM_001106549	Integrin, alpha V	Interacts with extracellular matrix proteins to mediate cell adhesion and play a role in cell migration. May regulate angiogenesis and cancer progression.
Itgax	XM_001080404	Integrin, alpha X	Involved in the adherence of neutrophils and monocytes to stimulated endothelium cells, and in the phagocytosis of complement coated particles.
Jag1	NM_019147	Jagged 1	Ligand for the receptor notch 1, which has been shown to play a role in hematopoiesis.
Kdr	NM_013062	Kinase insert domain receptor	Functions as the main mediator of VEGF-induced endothelial proliferation, survival, migration, tubular morphogenesis, and sprouting.
Lep	NM_013076	Leptin	Involved in regulation of body weight as well as regulation of immune and inflammatory responses, hematopoiesis, angiogenesis, and wound healing.
Lrp5	NM_001106321	Low density lipoprotein receptor-related protein 5	Plays a key role in skeletal homeostasis; many bone density related diseases are caused by mutations in this gene.
Ccl2	NM_031530	Chemokine (C-C motif) ligand 2	A chemokine that displays chemotactic activity for monocytes and basophils, but not for neutrophils or eosinophils.
Ccl3	NM_013025	Chemokine (C-C motif) ligand 3	Small inducible cytokine that plays a role in inflammatory responses through binding to the receptors CCR1, CCR4 and CCR5.
Mmp9	NM_031055	Matrix metallopeptidase 9	Involved in the breakdown of extracellular matrix in embryonic development, reproduction, tissue remodeling, and disease processes.

Myod 1	NM_176079	Myogenic differentiation 1	Regulates muscle cell differentiation by inducing cell cycle arrest, a prerequisite for myogenic initiation; is also involved in muscle regeneration.
Notch 1	NM_001105721	Notch homolog 1, translocation-associated (Drosophila)	Plays a role in a variety of developmental processes by controlling cell fate decisions.
Bglap	NM_013414	Bone gamma-carboxyglutamate (gla) protein	Also known as osteocalcin, a pro-osteoblastic noncollagenous protein found in bone and dentin; acts as a hormone involved in bone mineralization and calcium ion homeostasis.
Pou5f 1	NM_001009178	POU class 5 homeobox 1	Plays a key role in embryonic development and stem cell pluripotency.
Omd	NM_031817	Osteomodulin	Primarily expressed by osteoblasts; putative role in regulation of mineralization.
Spp1	NM_012881	Secreted phosphoprotein 1	Involved in the attachment of osteoclasts to the mineralized bone matrix; also acts as a cytokine, upregulating expression of interferon-gamma and interleukin-12.
Pdgfa	NM_012801	Platelet-derived growth factor alpha polypeptide	A mitogenic factor for cells of mesenchymal origin.
Phex	NM_013004	Phosphate regulating endopeptidase homolog, X-linked	Thought to be involved in bone and dentin mineralization and renal phosphate reabsorption.
Pparg	NM_013124	Peroxisome proliferator-activated receptor gamma	Acts as a transcription factor, regulating adipocyte differentiation.
Ptch1	NM_053566	Patched homolog 1 (Drosophila)	Acts as a receptor for sonic hedgehog, which is implicated in formation of embryonic structures and tumorigenesis. Functions as a tumor suppressor.
Ptk2	NM_013081	PTK2 protein tyrosine kinase 2	May be involved in cell growth and intracellular signal transduction pathways triggered in response to certain neural peptides or to cell interactions with the extracellular matrix.
Rhoa	NM_057132	Ras homolog gene family, member A	A small GTPase protein known to regulate the actin cytoskeleton in the formation of stress fibers.
Runx2	NM_053470	Runt-related transcription factor 2	Essential for osteoblastic differentiation and skeletal morphogenesis; acts as a scaffold for nucleic acids and regulatory factors involved in skeletal gene expression.
Scarb1	NM_031541	Scavenger receptor class B, member 1	Membrane receptor for high density lipoprotein cholesterol (HDL); mediates cholesterol transfer to and from HDL.
Smad3	NM_013095	SMAD family member 3	Functions as a transcriptional modulator activated by transforming growth factor-beta and is thought to play a role in the regulation of carcinogenesis.
Smo	NM_012807	Smoothened homolog (Drosophila)	A G protein-coupled receptor that interacts with the patched protein, a receptor for hedgehog proteins.
Smurf 1	NM_001109598	SMAD specific E3 ubiquitin protein ligase 1	Plays a key roll in the regulation of cell motility, cell signalling, and cell polarity.
Smurf 2	NM_001107061	SMAD specific E3 ubiquitin protein ligase 2	Interacts with SMAD1 and SMAD7 in order to trigger their ubiquitination and proteasome-dependent degradation.
Sox2	NM_001109181	SRY (sex determining region Y)-box 2	Required for stem-cell maintenance in the central nervous system; also regulates gene expression in the stomach.
Sox9	XM_001081628	SRY-box containing gene 9	Acts during chondrocyte differentiation and regulates transcription of the anti-Muellerian hormone (AMH) gene.
Sp1	NM_012655	Sp1 transcription factor	Transcription factor involved in cell differentiation, cell growth, apoptosis, immune responses, response to DNA damage, and chromatin remodeling.
Sp7	NM_181374	Sp7 transcription factor	Bone specific transcription factor required for osteoblast differentiation and bone formation.
Sparc	NM_012656	Secreted protein, acidic, cysteine-rich (osteonectin)	Required for calcification of collagen in bone; also involved in extracellular matrix synthesis and promotion of changes to cell shape.
Tbx5	NM_001009964	T-box 5	Transcription factor involved in the regulation of developmental processes; may play a role in heart development and specification of limb identity.
Tert	NM_053423	Telomerase reverse transcriptase	Plays a role in cellular senescence; normally repressed in postnatal somatic cells resulting in progressive shortening of telomeres.
Tgfb1	NM_021578	Transforming growth factor, beta 1	Regulates proliferation, differentiation, adhesion, migration, and other functions in many cell types.
Tgfb3	NM_013174	Transforming growth factor, beta 3	Involved in embryogenesis and cell differentiation.
Tnf	NM_012675	Tumor necrosis factor (TNF superfamily, member 2)	Involved in the regulation of a wide spectrum of biological processes including cell proliferation, differentiation, apoptosis, lipid metabolism, and coagulation.

Twist1	NM_053530	Twist homolog 1 (Drosophila)	Transcription factor implicated in cell lineage determination and differentiation.
Vegfa	NM_031836	Vascular endothelial growth factor A	Specifically acts on endothelial cells, mediating increased vascular permeability, inducing angiogenesis, promoting cell migration, and inhibiting apoptosis.
Wnt5a	NM_022631	Wingless-type MMTV integration site family, member 5A	Secreted signaling protein implicated in oncogenesis, regulation of cell fate, and patterning during embryogenesis.
Gusb	NM_017015	Glucuronidase, beta	Hydrolase that degrades glycosaminoglycans, including heparan sulfate, dermatan sulfate, and chondroitin-4,6-sulfate.
Gapdh	NM_017008	Glyceraldehyde-3-phosphate dehydrogenase/ Housekeeping Gene	Catalyzes the reversible oxidative phosphorylation of glyceraldehyde-3-phosphate in carbohydrate metabolism.
Rplp0	NM_022402	Ribosomal protein, large, P0	Encodes a ribosomal protein that is a component of the 60S subunit.
Actb	NM_031144	Actin, beta	A major constituent of the contractile apparatus and one of the two nonmuscle cytoskeletal actins.
B2m	NM_012512	Beta-2 microglobulin	A serum protein found in association with the major histocompatibility complex (MHC) class I heavy chain on the surface of nearly all nucleated cells.
Hprt1	NM_012583	Hypoxanthine phosphoribosyltransferase 1	Plays a central role in the generation of purine nucleotides through the purine salvage pathway.

Appendix 2

ORS 2017 abstract acceptance:

Palovarotene Treatment Suppresses Osteoprogenitor Cell Activity and Ectopic Bone Formation in a Trauma Induced Rodent Model of Heterotopic Ossification

Ammar T Qureshi[1], Jonathan G Seavey[1,2], Katherine E Cilwa[1], Allison M Tomasino[1], Wesley Bova[3], Cynthia Boehm[3], Erin M Sanders[1], Devaveena Dey[1], Jonathan A Forsberg[1,2], George Muschler[3] and Thomas A Davis[1,2]
[1]Regenerative Medicine Department, Naval Medical Research Center, Silver Spring, MD, [2] Department of Surgery, Uniformed Services University and the Walter Reed National Military Medical Center, Bethesda, MD, [3] Department of Biomedical Engineering, Cleveland Clinic, Cleveland, OH.

Disclosures: J.A.F is a consultant for Clementia Pharmaceuticals, Inc. The other authors have no financial or personal conflicts of interest to disclose.

ABSTRACT INTRODUCTION:
Blasts and high-energy projectiles cause the majority of modern war wounds. The physiological insults produced by blast overpressure trauma account for approximately 70% of all combat-related war injuries involving soft tissue, bone, and neurovascular structures. Acute wound failures and subsequent heterotopic ossification (HO) formation are related to multiple complex inter-related systemic and local inflammatory responses to blast-related traumatic injury. In comparison to the civilian trauma setting, trauma-induced HO is vastly more prevalent in the military setting, occurring in approximately 65% of amputations and nearly 62% of limb sparing procedures [1-3]. We have established and characterized a rat model of trauma-induced HO that incorporates the critical injury patterns commonly seen in human combat casualties specifically a blast injury, comminuted femur fracture, a thigh-crush and a transfemoral amputation through the zone of injury. In this model, radiographic evidence of ectopic bone development is measurable in 100% of injured rats with nominal mortality (< 2%). Treatment strategies to prevent combat-related HO has garnered a greater focus as current prophylaxis strategies used in civilian trauma, such as post-operative administration of non-steroidal anti-inflammatory drugs and external-radiation beam therapy can be contraindicated in patients who sustain systemic combat or blast-related trauma [2, 4, 5]. We postulate the microenvironment that supports ectopic bone development contains a dynamic composite of cells within an inflammatory, osteogenic and angiogenic milieu and scaffold of extracellular matrix, where osteogenic stem/progenitor cells thrive. Our investigative approach has shifted to therapeutic and prevention

strategies focused on identifying the origin and targeting progenitor cells towards altering the ectopic bone microenvironment that supports early ectopic bone development and progression. The retinoid signaling is important for chondrocyte maturation and endochondral bone formation [6]. Shimono et al. demonstrated in a mouse genetic model of fibrodysplasia ossificans progressiva (FOP), a rare untreatable genetic disorder of progressive extraskeletal ossification, that the retinoic acid receptor γ (RARγ) agonist Palovarotene effectively inhibits HO formation [7, 8] via suppression of chondrocyte maturation and early cartilage vascularization. In this study, we assessed the capacity of Palovarotene treatment to (1) block trauma-induced ectopic bone formation; (2) suppress local and systemic inflammatory responses; and (3) suppress osteogenic progenitor cell development (proliferation/expansion/differentiation) within the injury site.

METHODS:

A total of 84 adult male Sprague Dawley rats (450-500 g) were used. Using our established combat-injury model (blast overpressure of 120 ± 7 kPa from a shock tube, comminuted femoral fracture, one minute thigh crush injury and amputation through zone of injury), rats were treated with either 100µl of vehicle control (3% DMSO/corn oil) or Palovarotene (1.0 mg/kg) via oral gavage every other day for 14 days, starting at postoperative day 1 (POD-1). In an initial study arm, surgical sites were monitored longitudinally over 84 days for evidence of wound dehiscence and ectopic bone formation using MicroCT imaging to quantitate total new bone and ectopic bone (non-associated with cortical margins) volume. In a second study arm, serum was collected and assayed (Luminex multianalyte profiling) for various inflammatory mediators from cohorts of rats euthanized at PODs 1, 3, 7, 10, 14, and 21 (n=5 rats /treatment/time point). Next, soft tissue extracellular matrix collagen and mineralization at the distal portion of the residual limb was assessed by Raman Spectroscopy using a near infrared excitation Raman probe (Kaiser Optical Systems, Inc.). Spectra peak heights and peak areas were processed using in-house MATLAB® scripts. Expression of chondrogenic, angiogenic and osteogenic gene transcripts and osteogenic connective tissue progenitor cells (CTP-O) within the injured/healing muscle/soft tissue immediately surrounding the distal portion of the residual limb was determined by RT-PCR and osteogenic colony-forming cell assays (Colonyze™ image analysis software) under normoxic culture conditions (21% O_2), respectively.

RESULTS SECTION:

Palovarotene treatment significantly suppressed total new bone (16.2 ± 4.9 mm^3 to 5.3 ± 1.3 mm^3, p= 0.02; 67% mitigation) and ectopic bone (0.6 ± 0.4 mm^3 to 100% inhibition; p= 0.04) formation. Lower prevalence of osteogenic CTPs was measured in muscle tissue collected from Palovarotene-treated rats as compared to vehicle-treated rats. Moreover, the absolute number of CTP-O/gram of tissue was significantly decreased in Palovarotene-treated rats POD-7 (p =0.01) and POD-10 (p =0.049) (Figure 1). Consistent with these observations, Palovarotene treatment resulted in significantly reduced serum levels (IL-1α, IL-1β, IL-6, IL-10, IL-18, TNF-α, VEGF, G-CSF, GM-CSF; p<0.05) at POD-10 in comparison to vehicle control-treated rats. Palovarotene treatment, also, significantly suppressed the expression of several trauma-induced osteoblast specific genes (alkaline phosphatase, *ALPL*; p=0.02 at POD-1 and POD-7, bone morphogenic protein 2, *BMP2;* p=0.0001 at POD-3, bone morphogenic protein 4, *BMP4;* p=0.005 at POD-1, osteopontin, *OPN*; p=0.02 at POD-1 and p=0.04 on POD-7, Smad Ubiquitination Regulatory Factor 1; *SMURF1*; p=0.03 at POD-3 and Smad ubiquitination regulatory factor 2; *SMURF2;* p=0.03 at POD-1), chondrogenic specific genes (cartilage oligomeric matrix protein; *COMP*; p=0.001 at POD-1) and angiogenic specific genes (vascular endothelial growth factor-A; *VEGF-A*; p=0.01 at POD-1 and p=0.02 at POD-3, vascular permeability factor receptor 1; (*FLT1*; p=0.01 at POD-1, vascular permeability factor receptor 2; *KDR*; p=0.04 at POD-3, endoglin; *ENG*; p=0.002 at POD-1) and hypoxic inducing factor 1-α; *HIF-1α*; p=0.002 at POD-1). Lastly, Raman spectra of vehicle-treated rats exhibited an increasing trend of bone mineral signal relative to the spectral contribution of soft tissue with increasing time from injury, demonstrated by changes in the 958 cm^{-1}/(1439 cm^{-1}+1455 cm^{-1}) band area ratio. Palovarotene-treated rats exhibited similar trends up to POD-14, although decrease in overall magnitude compared to vehicle control, and a final reduction of bone mineral to soft tissue signal by POD 21.

Figure 1. Total yield of CTP-O/ gram of soft tissue in untreated and Palovarot

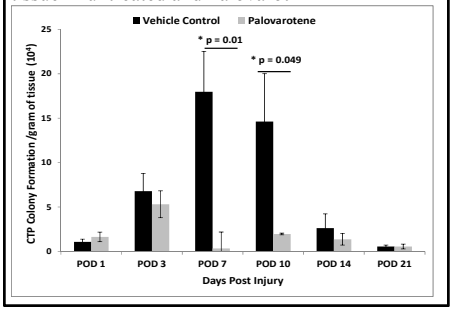

DISCUSSION:
We demonstrate that retinoid-dependent and retinoic acid receptor (RAR)-mediated mechanisms play a key role in trauma-induced ectopic endochondral bone formation. Palovarotene mediated mitigation of trauma-induced ectopic bone formation is associated with significantly reduced inflammatory, chondrogenic, angiogenic and osteogenic mediator signaling. In addition, Palovarotene treatment, when given the day after injury, reduced the local increase in the number of colony founding CTP-Os at 3, 7 and 10 days. This suggests a possible direct effect in inhibiting proliferation CTP-O progenitors as a mechanism underlining the drug's anti chondro-angio-osteogenic properties.

SIGNIFICANCE:
By preventing the HO formation completely, we aim to change our current paradigm of HO management from one of delayed diagnosis and surgical extirpation to one of primary prevention. This treatment may benefit injured service members with delayed evacuation given the opportunity to deploy prophylaxis in forward units.